Cell Reports

Report

NF45 and NF90 Regulate Mitotic Gene Expression by Competing with Staufen-Mediated mRNA Decay

Graphical Abstract

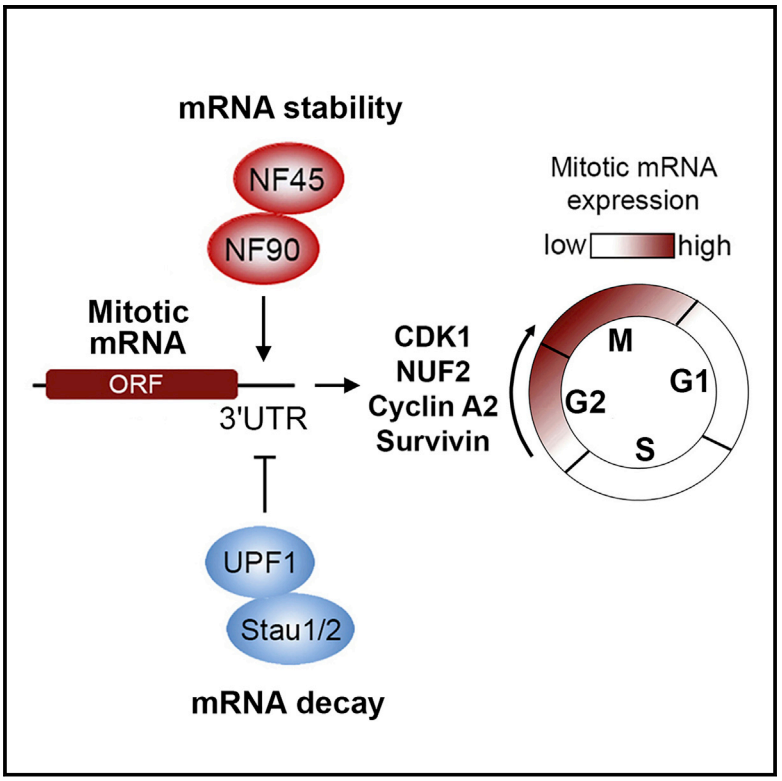

Highlights

- Depletion of NF45 or NF90 leads to pleiotropic mitotic defects
- The NF45-NF90 complex associates with, and regulates, a cluster of mitotic mRNAs
- The proximity interactome of NF45 and NF90 reveals Stau1 and Stau2
- Depletion of Stau1/2 rescues mitotic defects induced by loss of NF45 or NF90

Authors

Sami Nourreddine, Geneviève Lavoie, Justine Paradis, ..., Michel Bouvier, Sébastien Carreno, Philippe P. Roux

Correspondence

philippe.roux@umontreal.ca

In Brief

The timely expression of cell cycle genes is finely controlled by specific transcriptional programs. In this study, Nourreddine et al. evaluate the role of RNA-binding proteins in the post-transcriptional regulation of cell cycle genes. They show that the NF45-NF90 complex regulates the expression of an important cluster of mitotic mRNAs.

Nourreddine et al., 2020, Cell Reports *31*, 107660
May 19, 2020
https://doi.org/10.1016/j.celrep.2020.107660

CellPress

Cell Reports

CellPress
OPEN ACCESS

Report

NF45 and NF90 Regulate Mitotic Gene Expression by Competing with Staufen-Mediated mRNA Decay

Sami Nourreddine,[1] Geneviève Lavoie,[1] Justine Paradis,[2] Khaled Ben El Kadhi,[3] Antoine Méant,[1] Léo Aubert,[1] Benoit Grondin,[1] Patrick Gendron,[1] Benoit Chabot,[4] Michel Bouvier,[1,5] Sébastien Carreno,[1,6] and Philippe P. Roux[1,6,7,*]

[1]Institute for Research in Immunology and Cancer (IRIC), Université de Montréal, Montreal, QC H3T 1J4, Canada
[2]Moores Cancer Center, University of California, San Diego, La Jolla, CA 92037, USA
[3]Department of Biology, New York University, New York, NY 10003, USA
[4]Department of Microbiology and Infectious Diseases, Faculty of Medicine and Health Sciences, Université de Sherbrooke, Sherbrooke, QC J1H 5N4, Canada
[5]Department of Biochemistry and Molecular Medicine, Faculty of Medicine, Université de Montréal, Montreal, QC H3T 1J4, Canada
[6]Department of Pathology and Cell Biology, Faculty of Medicine, Université de Montréal, Montreal, QC H3T 1J4, Canada
[7]Lead Contact
*Correspondence: philippe.roux@umontreal.ca
https://doi.org/10.1016/j.celrep.2020.107660

SUMMARY

In human cells, the expression of ~1,000 genes is modulated throughout the cell cycle. Although some of these genes are controlled by specific transcriptional programs, very little is known about their post-transcriptional regulation. Here, we analyze the expression signature associated with all 687 RNA-binding proteins (RBPs) and identify 39 that significantly correlate with cell cycle mRNAs. We find that NF45 and NF90 play essential roles in mitosis, and transcriptome analysis reveals that they are necessary for the expression of a subset of mitotic mRNAs. Using proteomics, we identify protein clusters associated with the NF45-NF90 complex, including components of Staufen-mediated mRNA decay (SMD). We show that depletion of SMD components increases the binding of mitotic mRNAs to the NF45-NF90 complex and rescues cells from mitotic defects. Together, our results indicate that the NF45-NF90 complex plays essential roles in mitosis by competing with the SMD machinery for a common set of mRNAs.

INTRODUCTION

Progression through the cell cycle requires the periodic expression of ~1,000 genes, which are coordinated by phase-specific transcriptional programs (Whitfield et al., 2002). Some of the best examples are members of the E2F family (Dyson, 1998), which mediate the expression of genes necessary for S phase entry and DNA synthesis (Trimarchi and Lees, 2002). Although the transcriptional control of G1/S transition is well documented, corresponding events mediating G2/M transition are less understood (Lim and Kaldis, 2013). FoxM1 is a member of the forkhead box (Fox) superfamily of transcription factors (Hannenhalli and Kaestner, 2009; Myatt and Lam, 2007), and its target genes include essential regulators of mitosis and components of the spindle assembly checkpoint (SAC) (Sadasivam et al., 2012; Wonsey and Follettie, 2005). During the G2 phase, FoxM1 recruits a transcriptional co-activator, the histone deacetylase p300/CREB binding protein, which promotes the expression of genes responsible for driving mitotic entry (Laoukili et al., 2008). Despite the fact that the expression of almost half of cell cycle genes peaks in G2 and/or M phases (Whitfield et al., 2002), few transcription factors were shown to participate in G2/M transition, suggesting additional mechanisms of regulation.

RNA-binding proteins (RBPs) have emerged as essential regulators of gene expression (Hentze et al., 2018). Nuclear factor (NF) 45 and 90 are, respectively, encoded by the *ILF2* and *ILF3* genes and interact via their DZF (domain associated with zinc fingers) (Wolkowicz and Cook, 2012). NF90 also contains two double-stranded RNA-binding motifs (dsRBMs) and arginine-glycine-rich (RGG/RG) regions, which mediate nucleic acid binding (Masliah et al., 2013; Thandapani et al., 2013). NF90 regulates the stability of various transcripts, including those encoding interleukin-2 (IL-2), Tau, vascular endothelial growth factor (VEGF), and MyoD (Larcher et al., 2004; Shi et al., 2005; Vumbaca et al., 2008; Zhu et al., 2010). NF45 and NF90 are ubiquitously expressed in human tissues (Buaas et al., 1999) and are upregulated in several malignancies (Guo et al., 2012; Huang et al., 2014; Ni et al., 2015; Song et al., 2017; Wan et al., 2015). Genome-wide CRISPR-Cas9 screens revealed that *ILF2* and *ILF3* are essential fitness genes (Hart et al., 2015; Wang et al., 2015). Accordingly, depletion of NF45 or NF90 was shown to perturb the proliferation of various cell lines (Guan et al., 2008), but their exact mechanism of action remains elusive.

Here, we show that the NF45-NF90 complex plays an important role in mitotic progression and genomic stability. Depletion of NF45 or NF90 induces pleiotropic cell cycle defects, including chromosome mis-segregation and frequent failure of cytokinesis. Transcriptome analysis revealed that NF45 and NF90 are necessary for the expression of a cluster of mitotic mRNAs, which also associate with the NF45-NF90 complex. Using a

Please cite this article in press as: Nourreddine et al., NF45 and NF90 Regulate Mitotic Gene Expression by Competing with Staufen-Mediated mRNA Decay, Cell Reports (2020), https://doi.org/10.1016/j.celrep.2020.107660

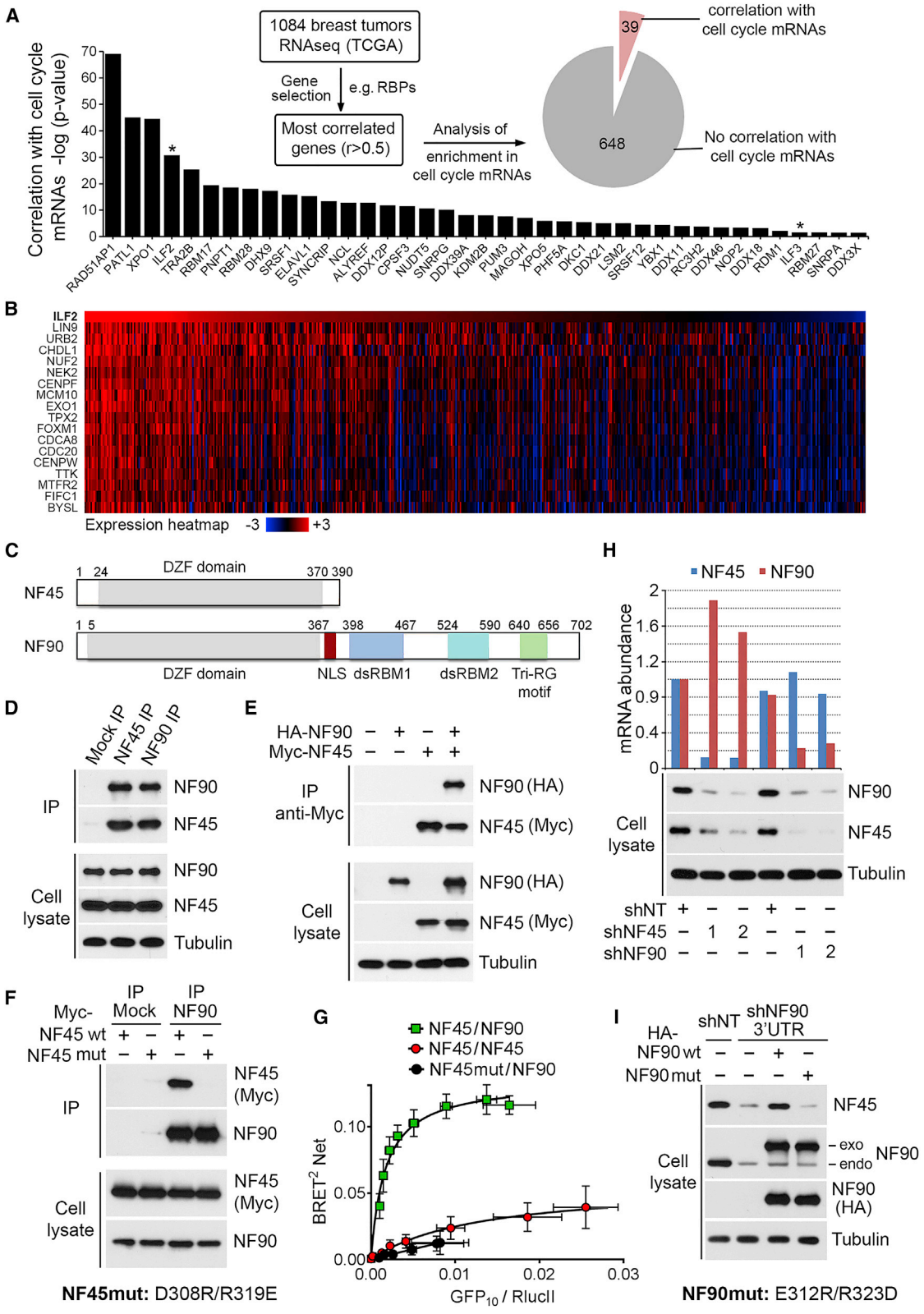

(legend on next page)

Please cite this article in press as: Nourreddine et al., NF45 and NF90 Regulate Mitotic Gene Expression by Competing with Staufen-Mediated mRNA Decay, Cell Reports (2020), https://doi.org/10.1016/j.celrep.2020.107660

proteomic approach to characterize the NF45-NF90 interactome, we identified several proteins involved in RNA metabolism, including Staufen-mediated mRNA decay (SMD). We found that the NF45-NF90 complex competes with SMD components to maintain the expression of mitotic mRNAs and promote mitotic progression.

RESULTS

NF45 and NF90 Form an RNA-Binding Complex that Correlates with Cell Cycle mRNAs

To identify RBPs that may be involved in the expression of cell cycle genes, we analyzed the mRNA signature associated with each of the 687 genes encoding proteins capable of binding RNA (KW-0694 from UniProt). We analyzed the most correlated genes ($r > 0.5$) for potential enrichment in cell cycle mRNAs (go.BP:0007049), which resulted in 39 RBPs (~5%) with significant values ($p > 0.05$; Figure 1A; Table S1). Among those, we identified HuR/*ELAVL1* ($p = 4.61 \times 10^{-16}$), *YBX1* ($p = 3.65 \times 10^{-5}$), and *DDX3X* ($p = 3.71 \times 10^{-2}$) as positive hits, which encode RBPs known to regulate the expression of several cell cycle genes (Kotake et al., 2017; Lai et al., 2010; Wang et al., 2000). We also identified *ILF2* ($p = 1.63 \times 10^{-31}$) and *ILF3* ($p = 2.42 \times 10^{-2}$), whose expression significantly correlates with cell cycle mRNAs (Figure 1B). These genes encode NF45 and NF90 (Figure 1C), respectively, which interact in cell via their DZF domains (Figures 1D and 1E). Mutations within the DZF domain of NF45 (D308R/R319E) prevent its association with NF90, as found by co-immunoprecipitation (Figure 1F) and using a bioluminescence resonance energy transfer (BRET) assay (Figure 1G). To address the reciprocal regulation of NF45 and NF90, both proteins were depleted using lentiviral vectors expressing short hairpin RNA (shRNA). Upon depletion of NF45 using two different shRNAs, we found a concomitant decrease in NF90 protein levels, despite mRNA levels being mostly unaffected by NF45 knockdown (Figure 1H). Similarly, we found that NF90 depletion reduced NF45 protein levels without negatively affecting its mRNA, suggesting that NF45 and NF90 mutually regulate their abundance in cells. To determine whether NF45 binding to NF90 was required for this co-regulation, we depleted cells with a shRNA construct targeting the 3′ untranslated region (3′ UTR) of the NF90 mRNA and expressed either wild-type (WT) NF90 or NF90 mutated in its DZF domain (E312R/R323D). Whereas WT NF90 was able to rescue NF45 levels upon endogenous NF90 depletion, we found that mutant NF90 could not (Figure 1I). NF45 binding to NF90 was previously shown to enhance double-stranded RNA (dsRNA) binding to NF90 by ~10-fold (Schmidt et al., 2017b), suggesting that NF45 might simultaneously regulate NF90 levels and function in cells. Together, these results demonstrate that NF45 and NF90 form a heterodimeric RNA-binding complex that may regulate the expression of cell cycle genes.

The NF45-NF90 Complex Is Required for Mitotic Progression and Cytokinesis

Consistent with previous findings (Guan et al., 2008), we found that depletion of NF45 or NF90 inhibits the proliferation of HeLa cells (Figure 2A). Although we did not detect major differences in the proportion of cells at each phase of the cell cycle, we observed an increase in polyploid cells (>4n) upon NF45 or NF90 depletion (Figures 2B and 2C). To understand the role of the NF45-NF90 complex in mitosis, we analyzed cells stably expressing tubulin-GFP using time-lapse microscopy. During cytokinesis, cells depleted for NF45 or NF90 show high cortical instability characterized by blebbing (Figure 2D; Videos S1 and S2). Mitotic cortical blebbing has been shown to be associated with cytokinesis failure (Birkenfeld et al., 2007; Charras et al., 2006). Consistent with this, we found that a large proportion of cells (~50%) depleted for NF45 or NF90 undergo cytokinesis failure characterized by cleavage furrow regression (Figures 2D and 2E; Video S2). In addition, we found a large proportion of mitotic cells undergoing cell death (~40%–50%; Figure 2F). These mitotic catastrophes occurred at different phases of mitosis, including metaphase (Video S3) or after cytokinesis (Video S4), which corresponds to different programs of mitotic catastrophe (Vitale et al., 2011).

To identify potential causes of cytokinesis defects, we analyzed chromosome segregation in cells depleted for NF45 or NF90. We found that chromosome alignment was severely impaired in NF45- or NF90-depleted cells, with ~45%–60% of metaphase cells showing one or more chromosomes outside of the metaphase plate (Figures 2G and 2H). These defects were almost always accompanied with asymmetric mitotic spindles of increased longitudinal lengths (Figures 2I and 2J),

Figure 1. NF45 and NF90 Form an RNA-Binding Complex that Correlates with Cell Cycle mRNAs

(A) Expression analysis between genes coding for RBPs (Nextprot ID KW-0694) and cell cycle genes (GO:0007049) from 1,084 breast tumor transcriptomes (The Cancer Genome Atlas [TCGA] breast adenocarcinoma). RBPs are classified according to the adjusted p value of the enrichment of cell cycle genes among correlated genes ($r > 0.5$).

(B) Expression heatmap showing the correlation between *ILF2* expression and a subset of cell cycle mRNAs.

(C) Schematic representation of NF45 and NF90 proteins, showing DZF (domain associated with zinc fingers), NLS (nuclear localization signal), dsRBM (double-stranded RNA binding motif), and Tri-RG motif (arginine-glycine-rich).

(D) Endogenous immunoprecipitation (IP) of NF90 and NF45 in HEK293 cells.

(E) Exogenous immunoprecipitation (IP) of NF90 and NF45 in HEK293 cells.

(F) HEK293 cells were transfected with Myc-tagged NF45 (WT or D308R/R319E), and endogenous NF90 was immunoprecipitated using an anti-NF90 antibody.

(G) BRET titration curves were performed in HEK293T cells transfected with a constant amount of NF90-RlucII or NF45-RlucII and increasing amounts of NF45 (WT or D308R/R319D)-GFP10. BRET400-GFP10 between NF90-RlucII or NF45-RlucII and NF45 (WT or D308R/R319D)-GFP10 was measured after the addition of coelenterazine-400a.

(H) HEK293 cells were depleted for NF45 or NF90 using two different shRNAs, and NF45/NF90 abundance was analyzed by immunoblotting and qPCR.

(I) HEK293 cells were depleted for endogenous NF90 using a shRNA targeting its 3′ UTR, and cells were transfected with HA-tagged NF90 (WT or E312R/R323D). Abundance of NF45 and NF90 was evaluated by immunoblotting.

Please cite this article in press as: Nourreddine et al., NF45 and NF90 Regulate Mitotic Gene Expression by Competing with Staufen-Mediated mRNA Decay, Cell Reports (2020), https://doi.org/10.1016/j.celrep.2020.107660

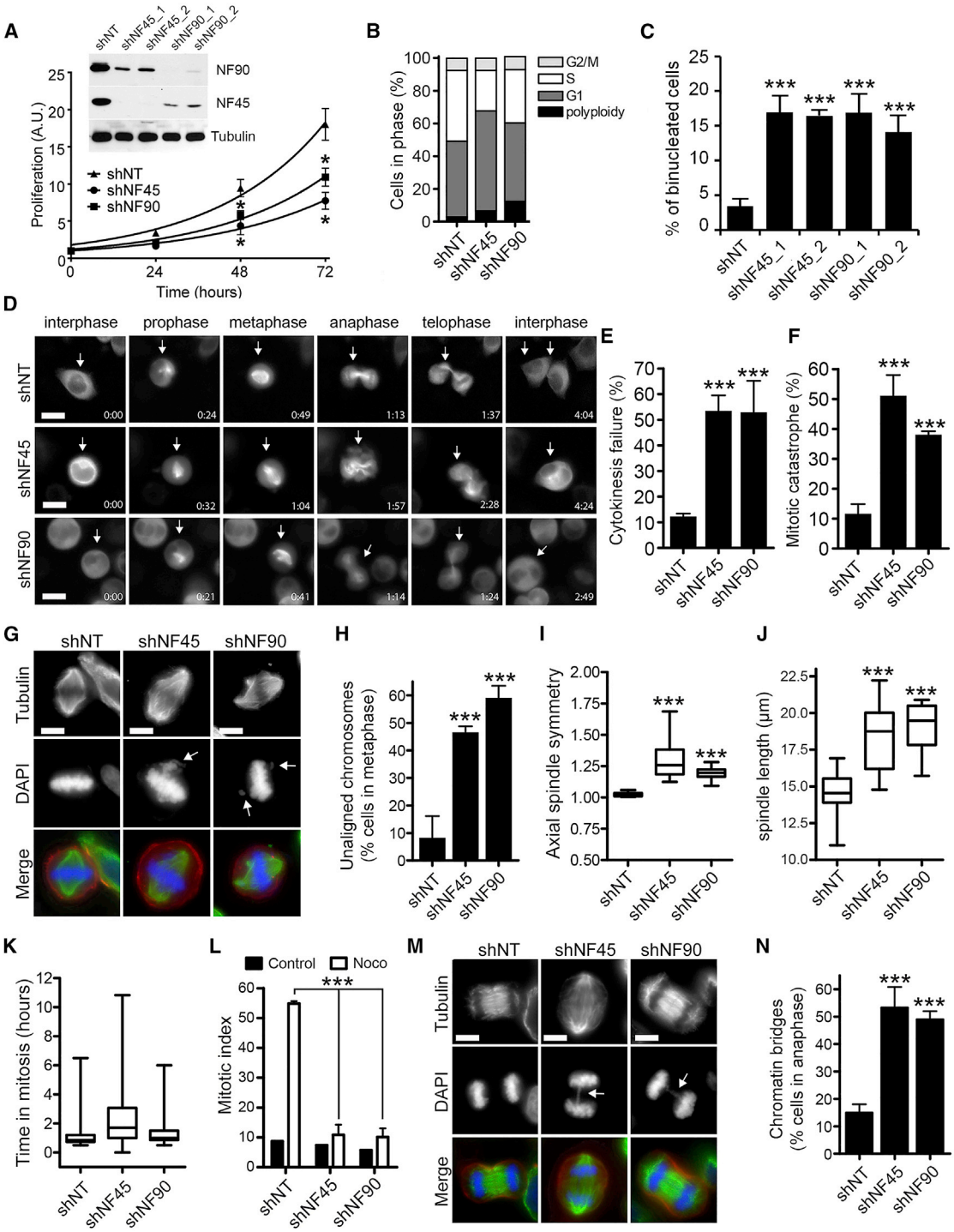

Figure 2. The NF45-NF90 Complex Is Required for Mitotic Progression and Cytokinesis

(A) Proliferation assay using WST-1 of HeLa cells with stable depletion of NF45 or NF90 over a 72-h time course. Data are expressed as the mean fold-change in optical density compared to the 0-h time point (A.U., arbitrary units).

(B) Fluorescence-activated cell sorting (FACS) analysis of DNA content of HeLa cells stably expressing shNT, shNF45, or shNF90. Data analysis and quantification of cells at different phase of the cell cycle were done using Flowjo.

(C) Quantification of binucleated cells by immunofluorescence in response to NF45 or NF90 depletion. A minimum of 1,500 cells per condition was quantified. ***$p < 0.001$ (two-tailed t test).

(legend continued on next page)

Please cite this article in press as: Nourreddine et al., NF45 and NF90 Regulate Mitotic Gene Expression by Competing with Staufen-Mediated mRNA Decay, Cell Reports (2020), https://doi.org/10.1016/j.celrep.2020.107660

suggestive of defective kinetochore-microtubule attachments (Bharadwaj et al., 2004; Goshima et al., 1999). When such defects occur, cells are halted by the SAC to prevent unequal separation of the genome in anaphase (Musacchio, 2015). Despite the presence of unaligned chromosomes in metaphase cells depleted for NF45 or NF90, the length of time in mitosis was not significantly affected under these conditions (Figure 2K), suggesting potential SAC defects. To test SAC functionality in the context of NF45 or NF90 depletion, we synchronized cells in mitosis using nocodazole and measured mitotic index by quantifying histone H3 phosphorylation at Ser10 by flow cytometry (Figure 2L). Although more than 50% of control cells were blocked in mitosis upon nocodazole treatment, only ~12% of cells depleted for NF45 or NF90 were positive for histone H3 phosphorylation. Consistent with potential SAC defects, we observed that a large proportion of NF45- or NF90-depleted cells (~50%) progressed to anaphase with visible chromatin bridges (Figures 2M and 2N). Altogether, these results show that depletion of the NF45-NF90 complex leads to pleiotropic mitotic defects, which likely contribute to polyploidy and/or mitotic catastrophe.

The NF45-NF90 Complex Regulates the Expression of a Cluster of Mitotic Genes

NF45 and NF90 have been implicated in different aspects of RNA metabolism, including transcription, mRNA stability, and translation (Barber, 2009; Castella et al., 2015). To identify mRNAs that may be regulated by the NF45-NF90 complex, we analyzed the impact of NF45 depletion on polyadenylated RNAs using transcriptome data from the ENCODE consortium (Diehl and Boyle, 2016). Interestingly, we found that NF45 depletion was associated with a >2-fold reduction in the levels of 86 mRNAs, including *ILF2* (Figure 3A; Table S2). As expected, *ILF3* levels were unaffected by NF45 depletion (Figure 3A). Using g:Profiler (Reimand et al., 2016), we analyzed NF45-sensitive transcripts for potential enrichments in biological functions. Strikingly, we found significant enrichments in several Reactome pathways (https://reactome.org/) related to mitosis (Figure 3B), including "mitotic cell cycle" ($p = 4.7 \times 10^{-6}$) and "sister chromatid cohesion" ($p = 1.3 \times 10^{-4}$). We represented significantly downregulated genes involved in the mitotic cell cycle using STRING (Figure 3C). Among this heavily connected cluster, we found genes coding for mitotic kinases (*CDK12*, *NEK2*, and *PLK1*), kinetochore proteins (*CENPE*, *CENPA*, and *NUF2*), members of the SAC (*BUB1*), and the chromosomal passenger complex (*BIRC5*). We selected four genes that play essential roles in mitotic progression and SAC activation (*NUF2*, *CDK1*, *CCNA2*, and *BIRC5*) and confirmed their sensitivity to NF45 and NF90 depletion at the mRNA level (Figure 3D). We also observed a decrease in proteins encoded by these genes in HeLa, MDA-MB-231, and BT-20 cells depleted for NF45 or NF90 (Figures 3E, 3F, and S1A). Consistent with this, we found that depletion of NF45 or NF90 in MDA-MB-231 and BT-20 cells resulted in pleiotropic mitotic defects (Figures S1B–S1F).

To determine whether the NF45-NF90 complex associates with mitotic mRNAs, we performed RNA-immunoprecipitation (RIP) assays on endogenous proteins (Figure 3G). We found that *NUF2*, *CDK1*, *CCNA2*, and *BIRC5* mRNAs were significantly enriched in endogenous NF45 or NF90 immunoprecipitates compared to control mRNAs, suggesting that the NF45-NF90 complex specifically associates with these mitotic mRNAs. To assess whether this association was dependent on the RNA-binding domains of NF90, we performed RIP assays on cells that ectopically express WT NF90 or NF90 lacking one (ΔRBM2) or both dsRBMs (ΔRBM1/2). We found that deletion of one but preferentially two dsRBMs significantly impaired mitotic mRNA enrichment compared to WT NF90 (Figure 3H). To determine whether the RNA-binding properties of NF90 are necessary for mitotic progression, we generated cells stably expressing WT NF90, NF90 ΔRBM2, or ΔRBM1/2 and assessed the effect of endogenous NF90 depletion on the frequency of binucleated cells (Figure 3I). Although we found that expression of WT NF90 rescues endogenous NF90 depletion, our results show that NF90 ΔRBM2 and ΔRBM1/2 do not reduce polyploidy (Figures 3J and 3K). These results indicate that the dsRBMs of NF90 are essential for its role in mitotic progression.

The NF45-NF90 Proximity Interactome Reveals a Functional Interplay with SMD Components

To identify potential interactors of the NF45-NF90 complex, we conducted a proximity-dependent biotin identification (BioID) screen in HEK293 cells (Roux et al., 2018). For this, NF45 (WT

(D) HeLa cells stably expressing tubulin-GFP (gray) and shNT, shNF45, or shNF90 were grown on glass-bottom culture dishes, followed by time-lapse imaging during 16 h. Arrows indicate cells undergoing mitosis. Scale bars: 25 μm.
(E) Quantification of cytokinesis failure in HeLa tubulin-GFP using time-lapse imaging. At least 100 cells per condition were analyzed. ***$p < 0.001$ (two-tailed t test).
(F) HeLa cells stably expressing shNT, shNF45, or shNF90 tubulin-GFP were followed by time-lapse imaging during 16 h, and cells undergoing mitotic catastrophe were quantified. At least 50 cells per condition were quantified. ***$p < 0.001$ (two-tailed t test).
(G) HeLa cells subjected to NF45 or NF90 depletion were stained for tubulin (green), F-actin (red), and DNA (blue) and imaged at 60× magnification. Arrows indicate unaligned chromosomes at metaphase. Scale bar: 10 μm.
(H) Quantification of cells having unaligned chromosomes in metaphase. At least 50 cells per condition were analyzed. ***$p < 0.001$ (two-tailed t test).
(I) Quantification of metaphase spindle axial symmetry toward the metaphase plate. At least 25 cells per condition were analyzed. ***$p < 0.0001$ (one-way ANOVA).
(J) Quantification of metaphase spindle length. At least 25 cells per condition were analyzed. ***$p < 0.0001$ (one-way ANOVA).
(K) HeLa tubulin-GFP cells were depleted for NF45 or NF90. Time in mitosis was determined using live-cell imaging by tracking cells in mitosis. At least 50 mitotic cells per condition were analyzed.
(L) HeLa cells depleted for NF45 or NF90 were treated with nocodazole for 16 h and then cells were stained for pH3-Ser10 and DNA (propidium iodide) and analyzed by FACS. The quantification shows the fraction of mitotic cells for each condition. ***$p < 0.001$ (two-tailed t test).
(M) HeLa cells were stained for tubulin (green), F-actin (red), and DNA (blue), and cells in anaphase were imaged at 60× magnification. Arrows indicate chromatin bridges. Scale bar: 10 μm.
(N) Quantification of chromatin bridges at anaphase. A minimum of 25 cells per condition were analyzed.

Please cite this article in press as: Nourreddine et al., NF45 and NF90 Regulate Mitotic Gene Expression by Competing with Staufen-Mediated mRNA Decay, Cell Reports (2020), https://doi.org/10.1016/j.celrep.2020.107660

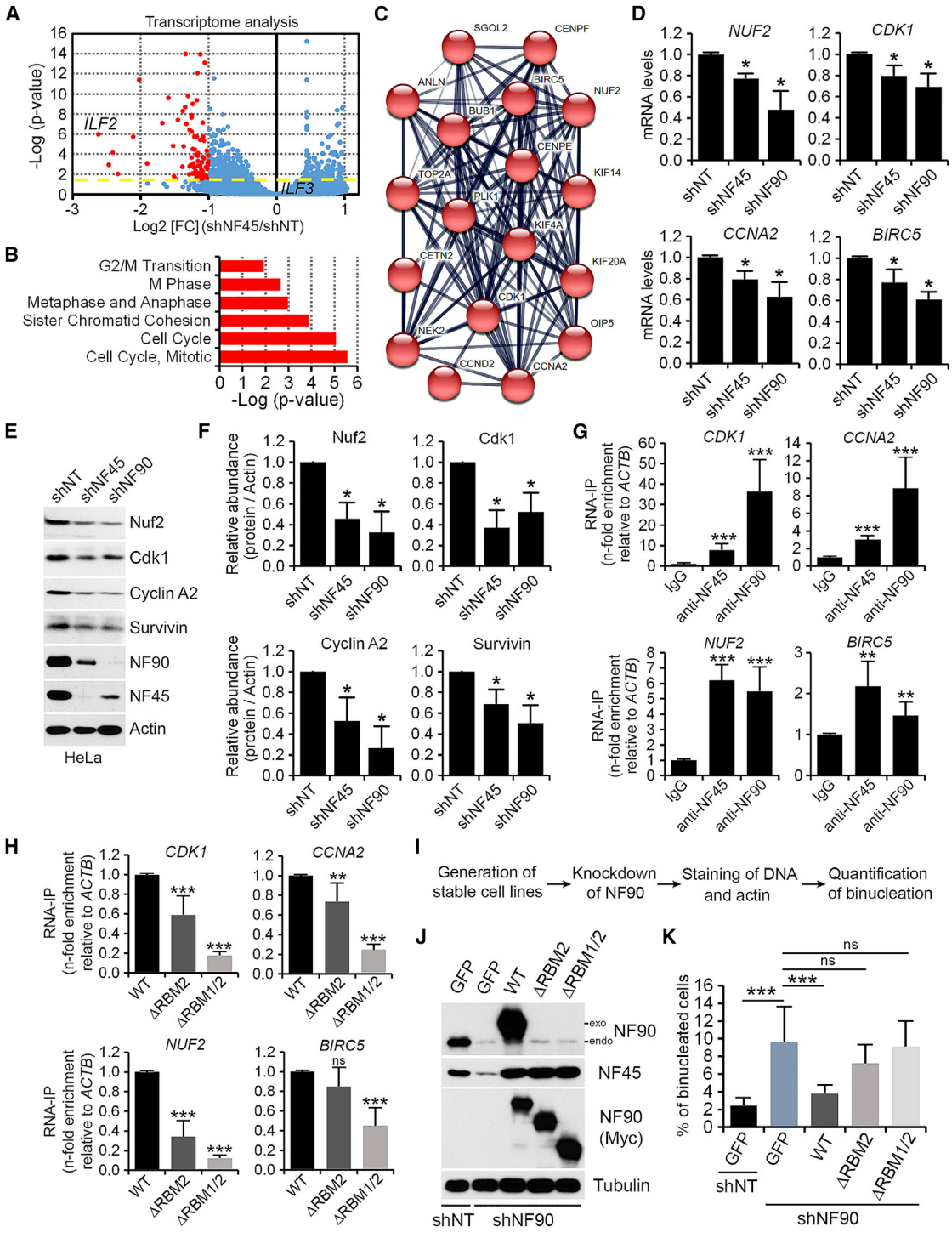

Figure 3. The NF45-NF90 Complex Regulates the Expression of a Cluster of Mitotic Genes

(A) Transcriptome analysis of HepG2 cells depleted for NF45/*ILF2*. Red dots indicate genes that are significantly depleted by more than 2-fold change compared to control.

(B) Classification of mRNAs significantly decreased in HepG2 cells depleted for NF45, based on Reactome Gene Ontology (GO) term enrichments associated with adjusted p values.

(C) Network representation of mitotic genes significantly decreased (>2-fold change) in response to NF45 depletion. Network edges represent functional interaction between these genes.

(legend continued on next page)

Please cite this article in press as: Nourreddine et al., NF45 and NF90 Regulate Mitotic Gene Expression by Competing with Staufen-Mediated mRNA Decay, Cell Reports (2020), https://doi.org/10.1016/j.celrep.2020.107660

and DZF mutant) and NF90 (WT and DZF mutant) were fused in frame with a promiscuous form (R118G) of the biotin ligase BirA (BirA*) (Figure 4A). Each bait was stably integrated in the tetracycline-inducible Flp-In T-Rex HEK293 cell system, and additional control cell lines (no BirA* and BirA*-GFP) were generated to enable data analysis. BioID coupled with mass spectrometry (MS) was performed in biological triplicates on these baits grown under standard conditions (Figure 4A). SAINTexpress (Teo et al., 2014) was used to define high-confidence proximity interactions, and only high-confidence interactions (SAINT $\geq$ 0.80) were considered further. Using this approach, we identified 63 and 83 prey proteins (false discovery rate [FDR] < 0.05; SAINT > 0.8) for WT NF45-BirA* and WT NF90-BirA*, respectively (Venn diagram in Figure 4A; Table S3). From these, 44 were found to be common to both baits, including known interactors of the NF45-NF90 complex, such as ZFR and PKR (EIF2AK2; Saunders et al., 2001; Wolkowicz and Cook, 2012). Using the DZF mutant (D308R/R319E) of NF45 as bait, we observed a large decrease in identified preys, whereas this was not the case with the DZF mutant of NF90 (E312R/R323D; dot plot in Figure 4A). These results suggest that the NF45 proximal interactome depends on NF90 binding but that NF90 does not require NF45 for interacting with most of its partners. Interestingly, most preys common to NF45 and NF90 are RNA-binding proteins that can be represented into four functional clusters, including RNA splicing ($p = 9.44 \times 10^{-15}$), ribosome biogenesis ($p = 8.56 \times 10^{-3}$), host immune response ($p = 1.6 \times 10^{-2}$), and mRNA stability ($p = 2.93 \times 10^{-4}$; Figure 4A). These results suggest that the NF45-NF90 complex regulates several aspects of RNA metabolism, including RNA splicing and stability.

To investigate whether the NF45-NF90 complex regulates mitotic RNA splicing, we performed alternative splicing PCR (ASPCR) and quantified the relative abundance of spliced isoforms in response to NF45 or NF90 depletion. For this, we have analyzed all mitotic genes found to be downregulated in the transcriptome of NF45-depleted cells (Figure 3C; Table S2) but did not find significant splicing alterations (Figure S2A). NF45 and NF90 are also known to regulate gene expression at the transcriptional level (Nakadai et al., 2015; Wu et al., 2018). To determine whether the NF45-NF90 complex regulates mitotic gene transcription, we performed luciferase assays using FoxM1 (6xDNA-binding motif) or *CDK1* (full promoter) reporters, which were validated using okadaic acid (Figures S3A and S3B; Alvarez-Fernández et al., 2011; Liu and Bird, 1998). Using these reporter assays, we found that overexpression or knockdown of NF45 or NF90 did not modulate *CDK1* promoter or FoxM1-dependent activities (Figures S3C–S3F), indicating that the NF45-NF90 complex does not regulate mitotic genes at the transcriptional level. The NF45-NF90 complex is known to regulate translation of *XIAP* and *cIAP1* (Faye et al., 2013). To test whether the NF45-NF90 complex affects translation of mitotic genes, we performed ribosome profiling in cells depleted for NF45 or NF90. These experiments did not reveal any translational regulation of mitotic genes by the NF45-NF90 complex (Figure S4).

In addition to RNA splicing components, we identified Stau1, Stau2, and UPF1 as proximity interactors of NF45 and NF90, which are components of the Staufen-mediated mRNA decay (SMD) machinery (Figure 4A). Stau1 and Stau2 are known to bind mRNAs via their 3′ UTR and to recruit the UPF1 helicase, leading to mRNA decay (Park and Maquat, 2013; Sakurai et al., 2017). We analyzed enhanced crosslinked immunoprecipitation (eCLIP) data for NF90 and UPF1 obtained from the ENCODE consortium (Figure S5) and found common coordinates in the 3′ UTR of several mitotic genes, such as *BIRC5*, *CDK1*, and *PLK1* (Figure S5C). Although ~30% of UPF1 peaks were found to intersect with NF90 peaks (Figure S5A), these results do not necessarily suggest the presence of common mRNA regions or sequence motifs. To confirm BioID results related to SMD components, we performed a streptavidin pull-down of biotinylated proteins. We confirmed that UPF1 is biotinylated in NF45-BirA* and NF90-BirA* cells, but not in control cells (Figure 4B). To further confirm these results, we immunoprecipitated endogenous UPF1 and determined the presence of endogenous NF45 and NF90, as well as hemagglutinin (HA)-tagged Stau1 (Figure 4C). We found that the NF45-NF90 complex co-immunoprecipitates with SMD components and that this interaction is sensitive to RNase A treatment, suggesting an RNA component to this interaction (Figure 4C). Consistent with previous findings (Kim et al., 2005), RNase A treatment did not disrupt the direct interaction between Stau1 and UPF1 (Figure 4C).

Interestingly, Stau1, Stau2, and NF90 possess dsRBMs, suggesting that they bind similar structures within target mRNAs. Stau1 overexpression was shown to negatively affect mitosis (Boulay et al., 2014), and Stau2 is important for spindle integrity in mouse oocytes (Cao et al., 2016). To assess whether Stau1 and/or Stau2 affect expression of mitotic mRNAs regulated by NF90, we performed qPCR in cells depleted for NF90 alone or in combination with Stau1 or Stau2 depletion (Figure 4D). We found that depletion of Stau1, and most importantly Stau2, rescued mitotic mRNA levels depleted by NF90 knockdown (Figure 4D), suggesting that Stau1/2 counteract NF90 in the regulation of mitotic mRNAs. To assess whether NF90 and Stau1/2

(D) HeLa cells were depleted for NF45 or NF90 using shRNAs, and *NUF2*, *CDK1*, *BIRC5*, and *CCNA2* mRNAs were quantified by qPCR. *p < 0.05 (two-tailed t test).

(E and F) HeLa cells were depleted for NF45 or NF90 using shRNAs. Abundance of NUF2, CDK1, survivin, and cyclin A2 were assessed by immunoblotting (E) and quantified over a minimum of 3 independent experiments (F). *p < 0.05 (two-tailed t test).

(G) Relative abundance of *NUF2*, *CDK1*, *CCNA2*, and *BIRC5* mRNAs immunoprecipitated with control immunoglobulin G (IgG), anti-NF45, or anti-NF90 antibodies, as measured by qPCR and normalized to the level of *ACTB*. **p < 0.01; ***p < 0.001 (two-tailed t test).

(H) HEK293 cells were transfected with Myc-tagged NF90 (WT, ΔRMB2, and ΔRBM1/2). The relative abundance of *NUF2*, *CDK1*, *CCNA2*, and *BIRC5* mRNAs immunoprecipitated with the anti-Myc antibody was then measured by qPCR.

(I) Schematic representation of the knockdown-rescue pipeline.

(J and K) HeLa cells were transduced with GFP or Myc-tagged NF90 (WT, ΔRMB2, and ΔRBM1/2), and endogenous NF90 was depleted using a shRNA targeting its 3′ UTR. Quantification of binucleated cells was done by analyzing at least 1,500 cells per condition (K). NF45 and NF90 abundance was assessed by immunoblotting (J). ***p < 0.001 (two-tailed t test).

Please cite this article in press as: Nourreddine et al., NF45 and NF90 Regulate Mitotic Gene Expression by Competing with Staufen-Mediated mRNA Decay, Cell Reports (2020), https://doi.org/10.1016/j.celrep.2020.107660

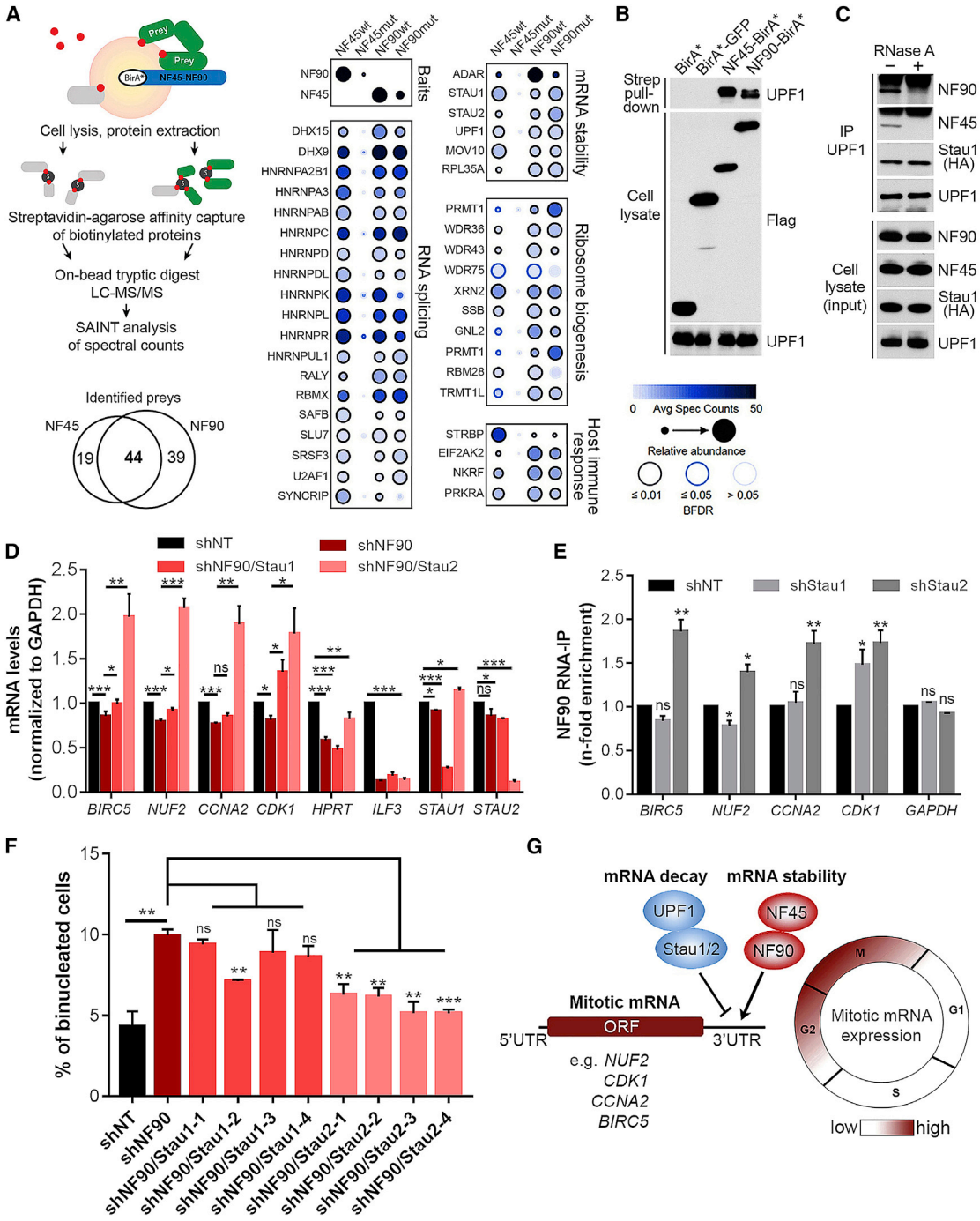

Figure 4. The Proximity Interactome of NF45 and NF90 Reveals a Functional Interplay with SMD Components

(A) Schematic representation of the BioID pipeline. Venn diagram showing common and respective preys identified for NF45 and NF90. Dot plot of proximity interactors for NF45 and NF90 is shown. All high-confidence proximity interactors are organized according to biological functions.

(B) HEK293 stably expressing inducible BirA*, BirA*-GFP, NF45-BirA*, and NF90-BirA* were induced with tetracycline and labeled with biotin during 24 h. Biotinylated proteins were precipitated using streptavidin beads, and UPF1 was detected using anti-UPF1 antibodies.

(C) HEK293 cells transfected with HA-tagged Stau1 were immunoprecipitated with endogenous UPF1 using anti-UPF1 antibody. Immunoprecipitates were treated or not with RNase A (10 μg/mL).

(D) qPCR of HeLa cells stably expressing shNT, shNF90, and combination of shNF90/shStau1 or shNF90/shStau2. *p < 0.05; **p < 0.01; ***p < 0.001 (two-tailed t test).

(E) Relative abundance of *NUF2*, *CDK1*, *CCNA2*, and *BIRC5* mRNAs immunoprecipitated with the anti-NF90 antibody in HEK293 cells stably expressing shNT, shStau1, or shStau2. *p < 0.05; **p < 0.01 (two-tailed t test).

(legend continued on next page)

Please cite this article in press as: Nourreddine et al., NF45 and NF90 Regulate Mitotic Gene Expression by Competing with Staufen-Mediated mRNA Decay, Cell Reports (2020), https://doi.org/10.1016/j.celrep.2020.107660

compete for binding to the same mRNAs, we performed RIP assays on endogenous NF90 from cells that were subjected to Stau1 or Stau2 depletion. Compared to control cells (shNT), we found that Stau2 depletion increased NF90 binding to *BIRC5*, *CCNA2*, *NUF2*, and *CDK1* mRNAs, although Stau1 depletion only increased *CDK1* binding (Figure 4E). These results suggest that the NF45-NF90 complex competes with SMD components for the expression of mitotic mRNAs. To determine the biological significance of these findings, we tested whether Stau1 or Stau2 knockdown (using 4 different shRNAs) could reverse the mitotic phenotype induced by NF90 depletion. We first quantified mRNA levels of *ILF3*, *STAU1*, and *STAU2* by qPCR (Figure S2B) and found that all shRNAs lead to knockdown of the targeted transcripts. Quantification of binucleated cells showed that shRNAs targeting Stau2 rescued the mitotic defects observed in NF90-depleted cells (Figure 4F). Together, these results suggest that the NF45-NF90 complex likely competes with the SMD machinery for the regulation of important mitotic mRNAs (Figure 4G).

DISCUSSION

In this study, we identified NF45 and NF90 as RBPs that regulate the expression of cell cycle mRNAs (Figure 1). We show that deregulation of the NF45-NF90 complex leads to pleiotropic mitotic defects (Figure 2) and that the NF45-NF90 complex alters expression of genes that are essential for mitotic progression (Figure 3). We find that the NF45-NF90 complex associates with mitotic mRNAs and that both dsRBMs of NF90 are required for mitotic fitness (Figure 3). Using BioID, we identify SMD components as proximity interactors of the NF45-NF90 complex and find that depletion of Stau2, and to a lesser extent Stau1, enhances the association of mitotic mRNAs to NF90 and rescues mitotic defects observed upon NF90 depletion (Figure 4). These results indicate that the NF45-NF90 complex competes with SMD components for mitotic mRNAs and thereby promotes mitotic progression (Figure 4G).

Our results indicate that the expression of 39 RBPs significantly correlates with cell cycle mRNAs (Figure 1). Among identified proteins, we found both NF45 and NF90, which form an obligate heterodimer in cells. Both proteins were shown to correlate with cell proliferation in various cellular contexts, including many tumor tissues (Guo et al., 2012; Hu et al., 2013; Huang et al., 2014; Jin et al., 2018; Ni et al., 2015; Wan et al., 2015; Yin et al., 2017). NF90 was shown to positively regulate *CCND1* and *CCNE1* mRNA stability and thereby promote G1/S transition (Jiang et al., 2015). Furthermore, genome-wide CRISPR screens have identified *ILF2* and *ILF3* as essential fitness genes in both immortalized and cancer cell lines (Hart et al., 2015; Wang et al., 2014), suggesting that they may be important therapeutic targets in cancer.

Our results show that the NF45-NF90 complex associates with several mitotic mRNAs in a dsRBM-dependent manner (Figure 3). dsRBMs are 65- to 70-amino-acid-long domains that recognize dsRNA via electrostatic interactions and structure complementarity rather than sequence-specific interaction (Masliah et al., 2013). NF90 tandem dsRBMs have been crystalized with synthetic dsRNA, which revealed that the interaction occurs on two RNA minor grooves separated by 10 bp (Masliah et al., 2013). Interestingly, NF45 binding to NF90 enhances dsRNA binding (Schmidt et al., 2017a), suggesting that NF90 dsRNA targets might be indirectly modulated by NF45. Using RIP arrays, two groups have determined the identity of mRNAs that interact with NF90 (Kuwano et al., 2008; Neplioueva et al., 2010), but results are quite divergent and may be explained by different methodologies. A recent study characterized the mRNA targets of the NF45-NF90 complex in mouse embryonic stem cells, which included many mRNAs encoding mitotic proteins (Ye et al., 2017). NF90 has been shown to be phosphorylated in mitotic cells (Matsumoto-Taniura et al., 1996; Smith and Miskimins, 2011), suggesting that specific mitotic kinases might regulate NF90 function. Altogether, these results indicate that the NF45-NF90 complex plays a ubiquitous role in mitosis, but more experimentation will be required to characterize the spectrum of mRNAs controlled by the NF45-NF90 complex.

SMD is a mammalian degradation process mediated by Stau1 or Stau2 binding to 3′ UTR dsRNA structures on mRNAs (Park and Maquat, 2013). Stau1 and Stau2 have been shown to be regulated during the G2/M phase of the cell cycle (Beaujois et al., 2017; Boulay et al., 2014), and ectopic Stau1 expression was shown to impair mitotic progression (Boulay et al., 2014), although Stau2 has been implicated in spindle integrity of mouse oocytes during meiosis (Cao et al., 2016). Here, we show that depletion of SMD components rescues the mitotic phenotype of NF90-depleted cells, suggesting a competition between both complexes. Besides their roles in mitosis, a broader relationship between SMD and the NF45-NF90 complex might exist. SMD is well known to play a role in myogenesis by negatively regulating the *MyoD* mRNA (de Morrée et al., 2017; Yamaguchi et al., 2008). Interestingly, NF90 knockout mice display impairments in skeletal muscle differentiation due to reduced MyoD expression (Shi et al., 2005). It would thus be interesting to determine whether this functional relationship exists in other functions regulated by SMD, including adipogenesis (Cho et al., 2012), apoptosis (Sakurai et al., 2017), and myogenesis (de Morrée et al., 2017; Yamaguchi et al., 2008).

STAR★METHODS

Detailed methods are provided in the online version of this paper and include the following:

- KEY RESOURCES TABLE
- RESOURCE AVAILABILITY
  - Lead Contact
  - Materials Availability
  - Data and Code Availability

(F) Quantification of binucleated cells expressing shNT, shNF90, and shNF90 combined with 4 different shRNAs targeting Stau1 or Stau2 by immunofluorescence. At least 1,000 cells per condition were quantified. *p < 0.05; **p < 0.01; ***p < 0.001 (two-tailed t test).
(G) Schematic model of the competition between the NF45-NF90 complex and Stau1/2-UPF1 complex for the regulation of mitotic fitness.

SUPPLEMENTAL INFORMATION

Supplemental Information can be found online at https://doi.org/10.1016/j.celrep.2020.107660.

ACKNOWLEDGMENTS

We are thankful to Dr. Luc Desgroseillers for providing Stau1 plasmid and antibodies and to Dr. Michael Mathews for providing NF45 and NF90 plasmids. We acknowledge the ENCODE consortium for transcriptomics and eCLIP data. This work was supported by grants from the Canadian Institutes for Health Research (MOP-142374 and PJT-152995 to P.P.R. and MOP-133683 to S.C. and B.C.) and the Natural Sciences and Engineering Research Council of Canada (P.P.R. and S.C.). P.P.R. is a scholar of the Fonds de la Recherche du Québec - Santé (FRQS). B.C. is the Pierre C. Fournier Chair in Functional Genomics. K.B.E.K. held a Ph.D. training award from the FRQS, a Ph.D. Fellowship Award from the Fondation Desjardins, and a Ph.D. Fellowship award from the Fondation du Grand Défi Pierre Lavoie.

AUTHOR CONTRIBUTIONS

S.N. designed and performed all experiments related to the phenotype induced by NF45 or NF90 depletion, the bioinformatic analysis revealing potential RBPs involved in cell cycle regulation, and wrote the manuscript. G.L. performed all immunoprecipitations, including RIP assays, as well as all DNA sub-cloning. J.P. designed and performed BRET experiments. L.A. participated in the experimental design and discussions related to the overall goals of the project. A.M. and B.G. performed all BioID experiments and data analysis. K.B.E.K. helped in the design and analysis of live-cell imaging experiments. P.G. performed the bioinformatic analysis of transcriptome data. S.C., M.B., and P.P.R. participated in study design and data analysis. P.P.R. and S.N. drafted and finalized the manuscript.

DECLARATION OF INTERESTS

The authors declare no competing interests.

Received: May 8, 2019
Revised: January 16, 2020
Accepted: April 28, 2020
Published: May 19, 2020

REFERENCES

Alvarez-Fernández, M., Halim, V.A., Aprelia, M., Laoukili, J., Mohammed, S., and Medema, R.H. (2011). Protein phosphatase 2A (B55α) prevents premature activation of forkhead transcription factor FoxM1 by antagonizing cyclin A/cyclin-dependent kinase-mediated phosphorylation. J. Biol. Chem. *286*, 33029–33036.

Anders, S., Pyl, P.T., and Huber, W. (2015). HTSeq–a Python framework to work with high-throughput sequencing data. Bioinformatics *31*, 166–169.

Barber, G.N. (2009). The NFAR's (nuclear factors associated with dsRNA): evolutionarily conserved members of the dsRNA binding protein family. RNA Biol. *6*, 35–39.

Beaujois, R., Ottoni, E., Zhang, X., Gagnon, C., Hassine, S., Mollet, S., Viranaicken, W., and DesGroseillers, L. (2017). The M-phase specific hyperphosphorylation of Staufen2 involved the cyclin-dependent kinase CDK1. BMC Cell Biol. *18*, 25.

Bharadwaj, R., Qi, W., and Yu, H. (2004). Identification of two novel components of the human NDC80 kinetochore complex. J. Biol. Chem. *279*, 13076–13085.

Birkenfeld, J., Nalbant, P., Bohl, B.P., Pertz, O., Hahn, K.M., and Bokoch, G.M. (2007). GEF-H1 modulates localized RhoA activation during cytokinesis under the control of mitotic kinases. Dev. Cell *12*, 699–712.

Boulay, K., Ghram, M., Viranaicken, W., Trépanier, V., Mollet, S., Fréchina, C., and DesGroseillers, L. (2014). Cell cycle-dependent regulation of the RNA-binding protein Staufen1. Nucleic Acids Res. *42*, 7867–7883.

Buaas, F.W., Lee, K., Edelhoff, S., Disteche, C., and Braun, R.E. (1999). Cloning and characterization of the mouse interleukin enhancer binding factor 3 (Ilf3) homolog in a screen for RNA binding proteins. Mamm. Genome *10*, 451–456.

Cao, Y., Du, J., Chen, D., Wang, Q., Zhang, N., Liu, X., Liu, X., Weng, J., Liang, Y., and Ma, W. (2016). RNA- binding protein Stau2 is important for spindle integrity and meiosis progression in mouse oocytes. Cell Cycle *15*, 2608–2618.

Castella, S., Bernard, R., Corno, M., Fradin, A., and Larcher, J.C. (2015). Ilf3 and NF90 functions in RNA biology. Wiley Interdiscip. Rev. RNA *6*, 243–256.

Charras, G.T., Hu, C.K., Coughlin, M., and Mitchison, T.J. (2006). Reassembly of contractile actin cortex in cell blebs. J. Cell Biol. *175*, 477–490.

Cho, H., Kim, K.M., Han, S., Choe, J., Park, S.G., Choi, S.S., and Kim, Y.K. (2012). Staufen1-mediated mRNA decay functions in adipogenesis. Mol. Cell *46*, 495–506.

Choi, H., Larsen, B., Lin, Z.Y., Breitkreutz, A., Mellacheruvu, D., Fermin, D., Qin, Z.S., Tyers, M., Gingras, A.C., and Nesvizhskii, A.I. (2011). SAINT: probabilistic scoring of affinity purification-mass spectrometry data. Nature methods *8*, 70–73.

de Morrée, A., van Velthoven, C.T.J., Gan, Q., Salvi, J.S., Klein, J.D.D., Akimenko, I., Quarta, M., Biressi, S., and Rando, T.A. (2017). Staufen1 inhibits MyoD translation to actively maintain muscle stem cell quiescence. Proc. Natl. Acad. Sci. USA *114*, E8996–E9005.

Diehl, A.G., and Boyle, A.P. (2016). Deciphering ENCODE. Trends Genet. *32*, 238–249.

Dyson, N. (1998). The regulation of E2F by pRB-family proteins. Genes Dev. *12*, 2245–2262.

Faye, M.D., Graber, T.E., Liu, P., Thakor, N., Baird, S.D., Durie, D., and Holcik, M. (2013). Nucleotide composition of cellular internal ribosome entry sites defines dependence on NF45 and predicts a posttranscriptional mitotic regulon. Mol. Cell. Biol. *33*, 307–318.

Goshima, G., Saitoh, S., and Yanagida, M. (1999). Proper metaphase spindle length is determined by centromere proteins Mis12 and Mis6 required for faithful chromosome segregation. Genes Dev. *13*, 1664–1677.

Guan, D., Altan-Bonnet, N., Parrott, A.M., Arrigo, C.J., Li, Q., Khaleduzzaman, M., Li, H., Lee, C.G., Pe'ery, T., and Mathews, M.B. (2008). Nuclear factor 45 (NF45) is a regulatory subunit of complexes with NF90/110 involved in mitotic control. Mol. Cell. Biol. *28*, 4629–4641.

Guo, Y., Fu, P., Zhu, H., Reed, E., Remick, S.C., Petros, W., Mueller, M.D., and Yu, J.J. (2012). Correlations among ERCC1, XPB, UBE2I, EGF, TAL2 and ILF3 revealed by gene signatures of histological subtypes of patients with epithelial ovarian cancer. Oncol. Rep. *27*, 286–292.

Hannenhalli, S., and Kaestner, K.H. (2009). The evolution of Fox genes and their role in development and disease. Nat. Rev. Genet. *10*, 233–240.

Hart, T., Chandrashekhar, M., Aregger, M., Steinhart, Z., Brown, K.R., MacLeod, G., Mis, M., Zimmermann, M., Fradet-Turcotte, A., Sun, S., et al. (2015). High-resolution CRISPR screens reveal fitness genes and genotype-specific cancer liabilities. Cell *163*, 1515–1526.

Hentze, M.W., Castello, A., Schwarzl, T., and Preiss, T. (2018). A brave new world of RNA-binding proteins. Nat. Rev. Mol. Cell Biol. *19*, 327–341.

Hu, Q., Lu, Y.Y., Noh, H., Hong, S., Dong, Z., Ding, H.F., Su, S.B., and Huang, S. (2013). Interleukin enhancer-binding factor 3 promotes breast tumor progression by regulating sustained urokinase-type plasminogen activator expression. Oncogene *32*, 3933–3943.

Huang, Q., He, X., Qiu, X., Liu, X., Sun, G., Guo, J., Ding, Z., Yang, L., Ban, N., Tao, T., and Wang, D. (2014). Expression of NF45 correlates with malignant grade in gliomas and plays a pivotal role in tumor growth. Tumour Biol. *35*, 10149–10157.

Jiang, W., Huang, H., Ding, L., Zhu, P., Saiyin, H., Ji, G., Zuo, J., Han, D., Pan, Y., Ding, D., et al. (2015). Regulation of cell cycle of hepatocellular carcinoma by NF90 through modulation of cyclin E1 mRNA stability. Oncogene *34*, 4460–4470.

Jin, Z., Xu, L., Zhang, L., Zhao, M., Li, D., Ye, L., Ma, Y., Ren, S., Yu, H., Wang, D., et al. (2018). Interleukin enhancer binding factor 2 is a prognostic biomarker for breast cancer that also predicts neoadjuvant chemotherapy responses. Am. J. Transl. Res. *10*, 1677–1689.

Julien, L.A., Carriere, A., Moreau, J., and Roux, P.P. (2010). mTORC1-activated S6K1 phosphorylates Rictor on threonine 1135 and regulates mTORC2 signaling. Mol. Cell. Biol. *30*, 908–921.

Kean, M.J., Couzens, A.L., and Gingras, A.C. (2012). Mass spectrometry approaches to study mammalian kinase and phosphatase associated proteins. Methods *57*, 400–408.

Keller, A., Nesvizhskii, A.I., Kolker, E., and Aebersold, R. (2002). Empirical statistical model to estimate the accuracy of peptide identifications made by MS/MS and database search. Anal. Chem. *74*, 5383–5392.

Kessner, D., Chambers, M., Burke, R., Agus, D., and Mallick, P. (2008). ProteoWizard: open source software for rapid proteomics tools development. Bioinformatics *24*, 2534–2536.

Kim, Y.K., Furic, L., Desgroseillers, L., and Maquat, L.E. (2005). Mammalian Staufen1 recruits Upf1 to specific mRNA 3'UTRs so as to elicit mRNA decay. Cell *120*, 195–208.

Kotake, Y., Arikawa, N., Tahara, K., Maru, H., and Naemura, M. (2017). Y-box binding protein 1 is involved in regulating the G_2/M phase of the cell cycle. Anticancer Res. *37*, 1603–1608.

Kuwano, Y., Kim, H.H., Abdelmohsen, K., Pullmann, R., Jr., Martindale, J.L., Yang, X., and Gorospe, M. (2008). MKP-1 mRNA stabilization and translational control by RNA-binding proteins HuR and NF90. Mol. Cell. Biol. *28*, 4562–4575.

Lai, M.C., Chang, W.C., Shieh, S.Y., and Tarn, W.Y. (2010). DDX3 regulates cell growth through translational control of cyclin E1. Mol. Cell. Biol. *30*, 5444–5453.

Laoukili, J., Alvarez, M., Meijer, L.A., Stahl, M., Mohammed, S., Kleij, L., Heck, A.J., and Medema, R.H. (2008). Activation of FoxM1 during G2 requires cyclin A/Cdk-dependent relief of autorepression by the FoxM1 N-terminal domain. Mol. Cell. Biol. *28*, 3076–3087.

Laoukili, J., Kooistra, M.R., Bras, A., Kauw, J., Kerkhoven, R.M., Morrison, A., Clevers, H., and Medema, R.H. (2005). FoxM1 is required for execution of the mitotic programme and chromosome stability. Nature cell biology *7*, 126–136.

Larcher, J.C., Gasmi, L., Viranaïcken, W., Eddé, B., Bernard, R., Ginzburg, I., and Denoulet, P. (2004). Ilf3 and NF90 associate with the axonal targeting element of Tau mRNA. FASEB J. *18*, 1761–1763.

Lim, S., and Kaldis, P. (2013). Cdks, cyclins and CKIs: roles beyond cell cycle regulation. Development *140*, 3079–3093.

Liu, H., and Bird, R.C. (1998). Characterization of the enhancer-like okadaic acid response element region of the cyclin-dependent kinase 1 (p34cdc2) promoter. Biochem. Biophys. Res. Commun. *246*, 696–702.

Liu, G., Zhang, J., Larsen, B., Stark, C., Breitkreutz, A., Lin, Z.Y., Breitkreutz, B.J., Ding, Y., Colwill, K., Pasculescu, A., et al. (2010). ProHits: integrated software for mass spectrometry-based interaction proteomics. Nat. Biotechnol. *28*, 1015–1017.

Love, M.I., Huber, W., and Anders, S. (2014). Moderated estimation of fold change and dispersion for RNA-seq data with DESeq2. Genome Biol *15*, 550.

Masliah, G., Barraud, P., and Allain, F.H. (2013). RNA recognition by double-stranded RNA binding domains: a matter of shape and sequence. Cell. Mol. Life Sci. *70*, 1875–1895.

Matsumoto-Taniura, N., Pirollet, F., Monroe, R., Gerace, L., and Westendorf, J.M. (1996). Identification of novel M phase phosphoproteins by expression cloning. Mol. Biol. Cell *7*, 1455–1469.

Mercier, J.F., Salahpour, A., Angers, S., Breit, A., and Bouvier, M. (2002). Quantitative assessment of beta 1- and beta 2-adrenergic receptor homo- and heterodimerization by bioluminescence resonance energy transfer. J. Biol. Chem. *277*, 44925–44931.

Musacchio, A. (2015). The molecular biology of spindle assembly checkpoint signaling dynamics. Curr. Biol. *25*, R1002–R1018.

Myatt, S.S., and Lam, E.W. (2007). The emerging roles of forkhead box (Fox) proteins in cancer. Nat. Rev. Cancer *7*, 847–859.

Nakadai, T., Fukuda, A., Shimada, M., Nishimura, K., and Hisatake, K. (2015). The RNA binding complexes NF45-NF90 and NF45-NF110 associate dynamically with the c-fos gene and function as transcriptional coactivators. J. Biol. Chem. *290*, 26832–26845.

Nepliouéva, V., Dobrikova, E.Y., Mukherjee, N., Keene, J.D., and Gromeier, M. (2010). Tissue type-specific expression of the dsRNA-binding protein 76 and genome-wide elucidation of its target mRNAs. PLoS ONE *5*, e11710.

Ni, S., Zhu, J., Zhang, J., Zhang, S., Li, M., Ni, R., Liu, J., Qiu, H., Chen, W., Wang, H., and Guo, W. (2015). Expression and clinical role of NF45 as a novel cell cycle protein in esophageal squamous cell carcinoma (ESCC). Tumour Biol. *36*, 747–756.

Park, E., and Maquat, L.E. (2013). Staufen-mediated mRNA decay. Wiley Interdiscip. Rev. RNA *4*, 423–435.

Reimand, J., Arak, T., Adler, P., Kolberg, L., Reisberg, S., Peterson, H., and Vilo, J. (2016). g:Profiler-a web server for functional interpretation of gene lists (2016 update). Nucleic Acids Res. *44* (*W1*), W83–W89.

Roux, P.P., Ballif, B.A., Anjum, R., Gygi, S.P., and Blenis, J. (2004). Tumor-promoting phorbol esters and activated Ras inactivate the tuberous sclerosis tumor suppressor complex via p90 ribosomal S6 kinase. Proc. Natl. Acad. Sci. USA *101*, 13489–13494.

Roux, K.J., Kim, D.I., Burke, B., and May, D.G. (2018). BioID: a screen for protein-protein interactions. Curr. Protoc. Protein Sci. *91*, 19.23.1–19.23.15.

Sadasivam, S., Duan, S., and DeCaprio, J.A. (2012). The MuvB complex sequentially recruits B-Myb and FoxM1 to promote mitotic gene expression. Genes Dev. *26*, 474–489.

Sakurai, M., Shiromoto, Y., Ota, H., Song, C., Kossenkov, A.V., Wickramasinghe, J., Showe, L.C., Skordalakes, E., Tang, H.Y., Speicher, D.W., and Nishikura, K. (2017). ADAR1 controls apoptosis of stressed cells by inhibiting Staufen1-mediated mRNA decay. Nat. Struct. Mol. Biol. *24*, 534–543.

Saunders, L.R., Perkins, D.J., Balachandran, S., Michaels, R., Ford, R., Mayeda, A., and Barber, G.N. (2001). Characterization of two evolutionarily

conserved, alternatively spliced nuclear phosphoproteins, NFAR-1 and -2, that function in mRNA processing and interact with the double-stranded RNA-dependent protein kinase, PKR. J. Biol. Chem. *276*, 32300–32312.

Schmidt, T., Friedrich, S., Golbik, R.P., and Behrens, S.E. (2017a). NF90-NF45 is a selective RNA chaperone that rearranges viral and cellular riboswitches: biochemical analysis of a virus host factor activity. Nucleic Acids Res. *45*, 12441–12454.

Schmidt, T., Knick, P., Lilie, H., Friedrich, S., Golbik, R.P., and Behrens, S.E. (2017b). The properties of the RNA-binding protein NF90 are considerably modulated by complex formation with NF45. Biochem. J. *474*, 259–280.

Schneider, C.A., Rasband, W.S., and Eliceiri, K.W. (2012). NIH Image to ImageJ: 25 years of image analysis. Nature methods *9*, 671–675.

Shi, L., Zhao, G., Qiu, D., Godfrey, W.R., Vogel, H., Rando, T.A., Hu, H., and Kao, P.N. (2005). NF90 regulates cell cycle exit and terminal myogenic differentiation by direct binding to the 3′-untranslated region of MyoD and p21WAF1/CIP1 mRNAs. J. Biol. Chem. *280*, 18981–18989.

Shteynberg, D., Deutsch, E.W., Lam, H., Eng, J.K., Sun, Z., Tasman, N., Mendoza, L., Moritz, R.L., Aebersold, R., and Nesvizhskii, A.I. (2011). iProphet: multi-level integrative analysis of shotgun proteomic data improves peptide and protein identification rates and error estimates. Mol. Cell. Proteomics *10*, M111.007690.

Smith, N.L., and Miskimins, W.K. (2011). Phosphorylation at serine 482 affects stability of NF90 and its functional role in mitosis. Cell Prolif. *44*, 147–155.

Song, D., Huang, H., Wang, J., Zhao, Y., Hu, X., He, F., Yu, L., and Wu, J. (2017). NF90 regulates PARP1 mRNA stability in hepatocellular carcinoma. Biochem. Biophys. Res. Commun. *488*, 211–217.

Teo, G., Liu, G., Zhang, J., Nesvizhskii, A.I., Gingras, A.C., and Choi, H. (2014). SAINTexpress: improvements and additional features in Significance Analysis of INTeractome software. J. Proteomics *100*, 37–43.

Thandapani, P., O'Connor, T.R., Bailey, T.L., and Richard, S. (2013). Defining the RGG/RG motif. Mol. Cell *50*, 613–623.

Trimarchi, J.M., and Lees, J.A. (2002). Sibling rivalry in the E2F family. Nat. Rev. Mol. Cell Biol. *3*, 11–20.

Vitale, I., Galluzzi, L., Castedo, M., and Kroemer, G. (2011). Mitotic catastrophe: a mechanism for avoiding genomic instability. Nat. Rev. Mol. Cell Biol. *12*, 385–392.

Vumbaca, F., Phoenix, K.N., Rodriguez-Pinto, D., Han, D.K., and Claffey, K.P. (2008). Double-stranded RNA-binding protein regulates vascular endothelial growth factor mRNA stability, translation, and breast cancer angiogenesis. Mol. Cell. Biol. *28*, 772–783.

Wan, C., Gong, C., Ji, L., Liu, X., Wang, Y., Wang, L., Shao, M., Yang, L., Fan, S., Xiao, Y., et al. (2015). NF45 overexpression is associated with poor prognosis and enhanced cell proliferation of pancreatic ductal adenocarcinoma. Mol. Cell. Biochem. *410*, 25–35.

Wang, W., Caldwell, M.C., Lin, S., Furneaux, H., and Gorospe, M. (2000). HuR regulates cyclin A and cyclin B1 mRNA stability during cell proliferation. EMBO J. *19*, 2340–2350.

Wang, T., Wei, J.J., Sabatini, D.M., and Lander, E.S. (2014). Genetic screens in human cells using the CRISPR-Cas9 system. Science *343*, 80–84.

Wang, T., Birsoy, K., Hughes, N.W., Krupczak, K.M., Post, Y., Wei, J.J., Lander, E.S., and Sabatini, D.M. (2015). Identification and characterization of essential genes in the human genome. Science *350*, 1096–1101.

Whitfield, M.L., Sherlock, G., Saldanha, A.J., Murray, J.I., Ball, C.A., Alexander, K.E., Matese, J.C., Perou, C.M., Hurt, M.M., Brown, P.O., and Botstein, D. (2002). Identification of genes periodically expressed in the human cell cycle and their expression in tumors. Mol. Biol. Cell *13*, 1977–2000.

Wolkowicz, U.M., and Cook, A.G. (2012). NF45 dimerizes with NF90, Zfr and SPNR via a conserved domain that has a nucleotidyltransferase fold. Nucleic Acids Res. *40*, 9356–9368.

Wonsey, D.R., and Follettie, M.T. (2005). Loss of the forkhead transcription factor FoxM1 causes centrosome amplification and mitotic catastrophe. Cancer Res. *65*, 5181–5189.

Wu, T.H., Shi, L., Adrian, J., Shi, M., Nair, R.V., Snyder, M.P., and Kao, P.N. (2018). NF90/ILF3 is a transcription factor that promotes proliferation over differentiation by hierarchical regulation in K562 erythroleukemia cells. PLoS ONE *13*, e0193126.

Yamaguchi, Y., Oohinata, R., Naiki, T., and Irie, K. (2008). Stau1 negatively regulates myogenic differentiation in C2C12 cells. Genes Cells *13*, 583–592.

Ye, J., Jin, H., Pankov, A., Song, J.S., and Blelloch, R. (2017). NF45 and NF90/NF110 coordinately regulate ESC pluripotency and differentiation. RNA *23*, 1270–1284.

Yin, Z.H., Jiang, X.W., Shi, W.B., Gui, Q.L., and Yu, D.F. (2017). Expression and clinical significance of ILF2 in gastric cancer. Dis. Markers *2017*, 4387081.

Zhu, P., Jiang, W., Cao, L., Yu, W., Pei, Y., Yang, X., Wan, B., Liu, J.O., Yi, Q., and Yu, L. (2010). IL-2 mRNA stabilization upon PMA stimulation is dependent on NF90-Ser647 phosphorylation by protein kinase Cbeta1. J. Immunol. *185*, 5140–5149.

Please cite this article in press as: Nourreddine et al., NF45 and NF90 Regulate Mitotic Gene Expression by Competing with Staufen-Mediated mRNA Decay, Cell Reports (2020), https://doi.org/10.1016/j.celrep.2020.107660

STAR★METHODS

KEY RESOURCES TABLE

REAGENT or RESOURCE	SOURCE	IDENTIFIER
Antibodies		
NF45	Bethyl	Cat# A303-147A, RRID:AB_10895652
NF90	Bethyl	Cat# A303-651A, RRID:AB_11204576
NUF2	Abcam	Cat# ab122962, RRID:AB_10902068
CDK1	Santa Cruz	Cat# sc-54, RRID:AB_627224
CCNA2	Santa Cruz	Cat# sc-53229, RRID:AB_782331
Survivin	Novus Biological	Cat# NB500-201, RRID:AB_10001517
Tubulin	Sigma-Aldrich	Cat# T5168, RRID:AB_477579
Actin	Sigma-Aldrich	Cat# A5441, RRID:AB_476744
Myc	Millipore	Cat# 05-419, RRID:AB_309725
UPF1	MBL International	Cat# RN108PW, RRID:AB_2616172
p-H3 Serine 10	Cell Signaling	Cat# 3377, RRID:AB_1549592
HA tag	Sigma-Aldrich	Cat# H6533, RRID:AB_439705
Mouse-HRP	Millipore	Cat# 71045-3, RRID:AB_10808067
Rabbit-HRP	Millipore	Cat# AP304P, RRID:AB_11212320
Tubulin Alexa Fluor 488	Thermo Fisher Scientific	Cat# 322588, RRID:AB_2532182
Bacterial and Virus Strains		
DH5α	Thermo Fisher Scientific	Cat# 18265017
Experimental Models: Cell Lines		
HeLa	ATCC	Cat# CCL-2, RRID:CVCL_0030
HEK293	ATCC	Cat# CRL-1573, RRID:CVCL_0045
HEK293T	ATCC	Cat# CRL-3216, RRID:CVCL_0063
MDA-MB-231	ATCC	Cat# CRL-12532, RRID:CVCL_0062
BT-20	ATCC	Cat# CRL-7912, RRID:CVCL_0178
Chemicals, Peptides, and Recombinant Proteins		
Nocodazole	Sigma-Aldrich	Cat# M1404
Thymidine	Sigma-Aldrich	Cat# T9250
Puromycin	Sigma-Aldrich	Cat# P8833
DAPI VECTASHIELD	Vector laboratories	Cat# H-1200
Coelenterazine-400a	Biotium	Cat# 10125
Polybrene	Sigma-Aldrich	Cat# S2667
WST-1	Sigma-Aldrich	Cat# 05 015 944 001
Propidium Iodide	Sigma-Aldrich	Cat# P4170
RNase A	Sigma-Aldrich	Cat# R6513
Cycloheximide	Sigma-Aldrich	
Biotin	Thermo Fisher Scientific	Cat# B1595
Tetracycline	Sigma-Aldrich	Cat# T7660
Hygromycin	Sigma-Aldrich	Cat# H3274
Protein A Sepharose	GE healthcare	Cat# 17-0780-01
Critical Commercial Assays		
RNeasy minikit	Quiagen	Cat# 74106
Secrete-Pair Gaussia Luciferase Assay Kit	Genecopeia	Cat# LF032
Luciferase Assay System	Promega	Cat# E1500

(*Continued on next page*)

Continued

REAGENT or RESOURCE	SOURCE	IDENTIFIER
Deposited Data		
shRNA ILF2 RNA-seq	ENCODE consortium	GEO:GSE88223
ILF3 eCLIP	ENCODE consortium	GEO:GSE91760
UPF1 eCLIP	ENCODE consortium	GEO:GSE91776
NF45 and NF90 BioID	This Paper	N/A
Oligonucleotides		
Primers for qPCR and ASPCR, see Table S4	This Paper	
Recombinant DNA		
pcDNA3-6Myc-NF45	This paper	
pcDNA5-FRT-Flag-BirA*-NF45	This paper	
pcDNA3-NF45-GFP10	This paper	
pcDNA3-NF45 D308R/R319D	This paper	
pcDNA5-FRT-Flag-BirA*-NF45 D308R/R319D	This paper	
pcDNA3-NF45 D308R/R319E-GFP10	This paper	
pLenti-6Myc-NF45	This paper	
pcDNA3-6Myc-NF90	This paper	
pcDNA5-FRT-Flag-BirA*-NF90	This paper	
pcDNA3-NF90-RLucII	This paper	
pcDNA3-NF90-GFP10	This paper	
pcDNA3-NF90 E312R/R323D	This paper	
pcDNA5-FRT-Flag-BirA*-NF90 E312R/R323D	This paper	
pcDNA3-NF90 E312R/R323D-GFP10	This paper	
pLenti-6Myc-NF90	This paper	
pLenti-6Myc-NF90 ΔRMB2	This paper	
pLenti-6Myc-NF90 ΔRMB1/2	This paper	
pKH3-HA-Stau1	Boulay et al., 2014	https://doi.org/10.1093/nar/gku506
pcDNA3-6xDB-FLuc	Laoukili et al., 2005	https://doi.org/10.1038/ncb1217
GLuc-SEAP-pEZX-PG04	Genecopeia	Cat# HPRM37184
pRSV-Rev	Addgene	Cat# 12253
pMDLg / pRRE	Addgene	Cat# 12251
pMD2- VSVG	Addgene	Cat# 12259
shRNA ILF2	Sigma-Aldrich	TRCN0000014553 TRCN0000329725
shRNA ILF3	Sigma-Aldrich	TRCN0000014578 TRCN0000014582
shRNA Stau1	Sigma-Aldrich	TRCN0000164920 TRCN0000166217 TRCN0000158514 TRCN0000159567
shRNA Stau2	Sigma-Aldrich	TRCN0000157149 TRCN0000153783 TRCN0000152870 TRCN0000178809
L304-EGFP-Tubulin-WT	Addgene	Cat# 64060
Software and Algorithms		
ImageJ	Schneider et al., 2012	https://imagej.nih.gov/ij/
SoftWoRx	GE healthcare	http://incelldownload.gehealthcare.com/bin/download_data/SoftWoRx/7.0.0/SoftWoRx.htm
ZEN blue	Zeiss	https://www.zeiss.fr/microscopie/produits/microscope-software/zen-lite/zen-2-lite-download.html
FACSDiva	BD Bioscience	https://www.bdbiosciences.com/us/instruments/research/software/flow-cytometry-acquisition/bd-facsdiva-software/m/111112/resourcestools
FlowJo v10	FlowJo	https://www.flowjo.com/solutions/flowjo/downloads

(*Continued on next page*)

Please cite this article in press as: Nourreddine et al., NF45 and NF90 Regulate Mitotic Gene Expression by Competing with Staufen-Mediated mRNA Decay, Cell Reports (2020), https://doi.org/10.1016/j.celrep.2020.107660

Continued

REAGENT or RESOURCE	SOURCE	IDENTIFIER
HTseq	Anders et al., 2015	https://doi.org/10.1093/bioinformatics/btu638
DESeq2	Love et al., 2014	https://doi.org/10.1186/s13059-014-0550-8
SAINT	Choi et al., 2011	https://doi.org/10.1038/nmeth.1541

RESOURCE AVAILABILITY

Lead Contact

Further information and requests for resources and reagents should be directed to and will be fulfilled by the Lead Contact, Philippe. P. Roux (philippe.roux@umontreal.ca).

Materials Availability

All unique/stable reagents generated in this study are available from the Lead Contact with a completed Materials Transfer Agreement.

Data and Code Availability

Original/source data for RNA-seq (Figure 3), eCLIP (Figure S5) in the paper are available at https://www.encodeproject.org/. Original/source data for BioID (Figure 4) in the paper is available in Table S3

EXPERIMENTAL MODEL AND SUBJECT DETAILS

HeLa, MDA-MB-231 and HEK293 cells were maintained at 37°C in Dulbecco's modified Eagle's medium (DMEM) (GIBCO) with 4.5 g/liter glucose supplemented with 5% fetal bovine serum (FBS) and antibiotics. BT-20 cells were maintained at 37°C in Alpha modified Eagle's Medium (Wisent) with 10% FBS and antibiotics.

METHOD DETAILS

DNA Constructs

The original plasmids encoding human NF45, NF90 (pCDNA3-NF45 and pCDNA3-NF90) and Stau1 (pKH3-HA-Stau1) were respectively obtained from Dr. Mathews (New Jersey Medical School, NJ, USA) and Dr. Degroseillers (Université de Montréal, QC, Canada). These DNA constructs were used as template for generating 6Myc-tagged NF45 WT, NF45 mut (D308R/R319D), NF90 WT, NF90 mut (E312R/R323D), NF90 ΔRMB2, NF90 ΔRBM1/2, Flag-tagged BirA*-NF45 WT, BirA*-NF45 mut (D308R/R319D), BirA*-NF90 WT, BirA*-NF90 mut (E312R/R323D) in the pcDNA3, pCDNA5-FRT and pLenti backbones. We obtained the 6xDB luciferase reporter (pcDNA3) from Dr. Medema (Netherland Cancer Institute, Amsterdam, Netherlands). We purchased the dual CDK1 promoter reporter (GLuc-SEAP-pEZX-PG04) from Genecopoeia (Rockville, MD, USA).

Immunoprecipitations and Immunoblotting

Cell lysates were prepared as previously described (Roux et al., 2004). Briefly, cells were washed three times with ice-cold phosphate-buffered saline (PBS) and lysed in BLB (10 mM K_3PO_4, 1 mM EDTA, 5 mM EGTA, 10 mM $MgCl_2$, 50 mM β-glycerophosphate, 0.5% Nonidet P-40, 0.1% Brij 35, 0.1% deoxycholic acid, 1 mM sodium orthovanadate [Na_3VO_4], 1 mM phenylmethylsulfonyl fluoride, and a cOmplete protease inhibitor cocktail tablet (Roche). For immunoprecipitations, cell lysates were incubated with the indicated antibodies for 2 h, followed by 1 h of incubation with protein A–Sepharose CL-4B beads (GE Healthcare). Immunoprecipitates were washed three times in lysis buffer, and beads were eluted and boiled in 2 × reducing sample buffer (5 × buffer is 60 mM Tris-HCl [pH 6.8], 25% glycerol, 2% SDS, 14.4 mM 2-mercaptoethanol, and 0.1% bromophenol blue). Eluates and total cell lysates were subjected to 10 to 12% SDS-PAGE, and resolved proteins were transferred onto polyvinylidene difluoride (PVDF) membranes for immunoblotting. The data presented are representative of results from at least three independent experiments.

Bioluminescence Resonance Energy Transfer (BRET) Assays

BRET assays were performed as described previously (Mercier et al., 2002). For BRET400-GFP10, proteins were fused to RLucII (donor) and GFP10 (acceptor). Coelenterazine-400a (coel-400a) (Biotium) was used as the luciferase substrate to generate light with a maximal emission peak at 400 nm, allowing GFP10 excitation (maximum at 400 nm). BRET was measured using a Mithras LB940 Multimode Microplate Reader (Berthold Technologies) equipped with either a BRET480-YFP filter set (donor 480 ± 20 nm and acceptor 530 ± 20 nm filters) or a BRET400-GFP10 filter set (donor 400 ± 70 nm and acceptor 515 ± 20 nm filters). Briefly, cells were seeded the day after transfection in a poly-L-ornithine (Sigma-Aldrich)–pretreated 96-well microplate (CulturePlate;

PerkinElmer Inc.). BRET values were collected after the addition of the luciferase substrate at a final concentration of 2.5 μM. BRET signals were determined as the ratio of the light emitted by acceptor (YFP or GFP10) over donor (RLuc or RLucII).

RNA-Immunoprecipitation (RNA-IP)

Cells were washed with ice-cold PBS and lysed in RIP buffer (50 mM Tris-HCl at pH 7.4, 300 mM NaCl, 1 mM $MgCl_2$, 0.05% NP-40, 1 mM Na_3VO_4, 1 mM PMSF, 1 mM DTT, 200 U/mL RNase Out, 100 μg/mL yeast tRNA (Sigma), cOmplete protease inhibitors. For immunoprecipitations, cell lysates were precleared with protein A-Sepharose beads for 30 min and then incubated with the indicated antibody for 2 h, followed by 1 h of incubation with protein A-Sepharose beads. Immunoprecipitates were washed six times with RIP buffer and divided for immunoblotting and RNA extraction. RNA was eluted twice with elution buffer (PK; 50 mM Tris-HCl at pH 7.4, 100 mM NaCl, 10 mM EDTA, 1% SDS, 5 mM DTT, 400 U/mL RNase Out, 0.25 μg/mL yeast) during 15 min at 65°C and digested with 4 mg/mL proteinase K (Roche) for 40 min at 37°C. RNA was then extracted with phenol-chloroform.

Reagents and Antibodies

Anti-NF45 (Bethyl), Anti-N90 (Bethyl), Anti-NUF2 (Abcam), Anti-CDK1 (Santa Cruz), Anti-Cyclin A2 (Santa Cruz), Anti-Survivin (Novus Biologicals), Anti-Tubulin (Sigma-Aldrich), Anti-Actin (Sigma-Aldrich), Anti-Myc (Sigma-Aldrich), Anti-UPF1 (MBL), phosphor-H3 Ser10 (Cell Signaling), Nocodazole (Sigma-Aldrich), Puromycin (Sigma-Aldrich), DAPI vectashield (Vectorlabs), TexasRed-Phalloidin (Invitrogen). All secondary horseradish peroxidase (HRP)-conjugated antibodies used for immunoblotting were purchased from Chemicon.

RNAi and Viral Infections

For shRNA-mediated knockdown of NF45 or NF90, lentiviruses were produced using vectors from the Mission TRC shRNA library (Sigma-Aldrich) targeting NF45 (TRCN0000014553, TRCN0000329725), NF90 (TRCN0000014578, TRCN0000014582), Stau1 (TRCN0000164920, TRCN0000166217, TRCN0000158514, TRCN0000159567), and Stau2 (TRCN0000157149, TRCN0000153783, TRCN0000152870, TRCN0000178809). Cells were infected in the presence of 4 μg/mL polybrene (Sigma-Aldrich), and, 3 d after viral infection, HeLa, MDA-MB-231 and BT-20 cells were treated and respectively selected with 2, 1.5 and 2 μg/mL puromycin.

Immunofluorescence Microscopy

For immunofluorescence analyses, 6×10^4 HeLa cells were seeded in 24-well plates containing coverslips. Twenty-four hours later, cells were fixed in 3.7% formaldehyde for 10 min. Cells were washed twice in PBS, permeabilized for 5 min in PBS containing 0.3% Triton X-100 and blocked with PBS containing 1% bovine serum albumin for 1h. Cells were incubated for 30min with anti-tubulin Alexa488 (Invitrogen), Phalloidin-Texas Red (Invitrogen) antibodies. Cells were stained with DAPI Vectashield (VectorLabs). Images were acquired on a DeltaVision microscope (Olympus U Plan S-Apo × 60 aperture) using softWoRx software equipped with a camera (CoolSNAP HQ2).

Transfections

HEK293 cells were transfected by calcium phosphate precipitation as previously described (Roux et al., 2004).

Live-cell Imaging

Five x 10^4 cells were seeded in 8-well Open μ-Slide (Ibidi, GmbH) and allowed to adhere overnight. Cells were filmed at 37°C with a DeltaVision microscope (Olympus U Plan S-Apo × 20/0.75 numerical aperture) using softWoRx software equipped with a camera (CoolSNAP HQ2). Images were acquired every 10 min for 18 h. Image analysis was done with softWoRx and ImageJ softwares.

Proliferation Assays

For proliferation assays, HeLa cells were grown in medium supplemented with 5% FBS. The relative number of viable cells was measured every 24 h during four consecutive days using the 2-(4-Iodophenyl)-3-(4-nitrophenyl)-5-(2,4-disulfophenyl)-2H-tetrazolium, inner salt (WST-1), cell proliferation assay from Roche, as shown elsewhere (Julien et al., 2010). The absorbance was measured at 490 nm using a Tecan GENios Plus microplate reader, and the results displayed represent the mean of triplicates ± standard error (SE).

Synchronization and Flow Cytometric Analysis of Cell Cycle Distribution

HeLa cells were synchronized in mitosis with a double thymidine block followed by nocodazole (Sigma-Aldrich) treatment for 18 h. Twenty-four hours after being seeded, cells were exposed to 2 mM thymidine (Sigma Aldrich) for 16 h. Cells were then released for 6 h followed by a second thymidine block for a further 16 h, then HeLa cell were incubated overnight with nocodazole at 1.5 μM. The DNA and RNA intercalating fluorescent dye propidium iodide (Sigma-Aldrich) was used to quantify cellular DNA content and cell cycle distribution. After treatment, HeLa cells were harvested and fixed in 95% ethanol at −20 °C. Before analysis, cells were incubated with RNase A (100 μg/ml; Sigma-Aldrich) and stained with propidium iodide (40 μg/ml) for 30 min. Samples were immediately analyzed by flow cytometry with a BD FACSCanto II flow cytometer (BD Biosciences) at low flow rate. A total of 2×10^4 events was recorded per sample, and the cell fraction G0/G1, S and G2/M phases were quantified with BD FACSDiva software (BD Biosciences) and plots were done with FlowJo.

Please cite this article in press as: Nourreddine et al., NF45 and NF90 Regulate Mitotic Gene Expression by Competing with Staufen-Mediated mRNA Decay, Cell Reports (2020), https://doi.org/10.1016/j.celrep.2020.107660

RNA-sequencing (RNA-Seq)

Transcriptome datasets were obtained from the Encyclopedia of DNA Elements (ENCODE) consortium (ILF2 shRNA knockdown in HepG2 cells followed by RNaseq: ENCSR366FFV; Control shRNA against no target in HepG2 cells followed by RNaseq: ENCSR305XWT). Gene expression were quantified using HTseq count from the alignment files created by STAR. DESeq2 version 1.10.1 was then used to identify differentially expressed genes using a Wald test.

Analysis of TCGA Datasets

Using Nextprot (https://www.nextprot.org/), we downloaded a list of annotated RNA-binding proteins (KW-0694), consisting of 687 entries. Using cBioPortal (https://www.cbioportal.org), we analyzed the TCGA breast invasive carcinoma dataset (1084 tumors) and extracted the mRNAs most correlated to each mRNA encoding RNA-binding proteins ($r \geq 0.5$). Using gProfiler (https://biit.cs.ut.ee/gprofiler/), we assessed the statistical significance of GO term enrichments (Cell cycle; GO:0007049) within the lists of co-expressed mRNAs.

RNA Extraction and Quantitative Real-Time PCR

Total RNA from cells was extracted by using the RNeasy minikit (QIAGEN). Total RNA was reverse transcribed by using a cDNA reverse transcription kit (Applied Biosystems) according to the manufacturer's instructions. Gene expression levels of the endogenous controls glyceraldehyde-3-phosphate dehydrogenase (*GAPDH*) and beta-actin (*ACTB*) were determined by using pre-validated TaqMan gene expression assays (Applied Biosystems). Expression levels of queried and control genes were determined by using assays designed with the Universal Probe Library (UPL) from Roche. PCRs were performed on an ABI Real Time 7900HT cycler and analyzed with SDS 2.2 software. Quantitative real-time PCR (qRT-PCR) was performed with TaqMan gene expression master mix (Applied Biosystems), and all samples were tested in duplicate. mRNA levels of queried genes were normalized to the averaged levels of both *GAPDH* and *ACTB*.

Alternative Splice Isoform PCR (ASPCR)

RT-PCR were performed by the RNomics Platform of the Université de Sherbrooke. Primers are listed below. Reverse transcription was done using 10 U of Transcriptor reverse transcriptase, 20 U of RNaseOUT (Invitrogen), 3.2 μg of random hexamers, 1 μM of dNTPs mix, 1 X Transcriptor RT reaction buffer and 0.2 – 2 μg of total RNA. PCR was done using 0.2 U of Platinium Taq, 0.6 μM of primers, 1.5 mM of MgCl2, 10 ng of cDNA template, 1X of PCR buffer and 200 μM of dNTPs mix. PCR reactions were performed on thermocyclers GeneAmp PCR System 9700 (Thermo Scientific-Invitrogen). A first cycle of 15 min at 95 °C was followed by 35 cycles of 30 s at 94 °C, 30 s at 55 °C, and 1 min at 72 °C. The reaction was ended with the extension step of 10 min at 72 °C. Visualization and analysis of amplified products were done using automated chip-based microcapillary electrophoresis on Labchip GX Touch HT instruments (Perkin Elmer).

Polysomal mRNA Profiling

Sucrose gradient velocity sedimentation was used to isolate the monosomal and polysomal fractions. For experiments using NF45 or NF90-depleted cells, following selection with puromycin, cells were passaged once in 15-cm dishes and then maintained in DMEM containing 5% serum and puromycin. HeLa NF45 or NF90-depleted cells were seeded in 15-cm dishes; 24 h later, fresh medium without puromycin was added, and cells were grown for another 24 h prior to harvesting. Ten minutes before harvesting, 100 μg/mL cycloheximide was added to the culture medium. Cells were washed in ice-cold PBS supplemented with 100 μg/mL cycloheximide and collected in polysome lysis buffer (PLB; 15 mM Tris at pH 7.4, 250 mM NaCl, 15 mM MgCl2, 1% Triton X-100, 100 μg/mL cycloheximide, 1 mM DTT, 400 U/mL RNase Out [Invitrogen, Life Technologies], protease inhibitors.) Samples were centrifuged at 10,000 × g for 10 min at 4°C. Protein concentration in the resulting supernatants was measured using the Bradford method, and equal amounts of protein were layered on a 20%–50% linear sucrose gradient and centrifuged in a Beckman SW41Ti rotor at 92,000 × g for 3 h at 4°C. Following centrifugation, the absorbance at 254nm was continuously monitored and recorded using a Gradient Station IP (Biocomp) attached to a UV-MII (GE Healthcare) spectrophotometer. Polysomal fractions were collected, and RNA was extracted using RNeasy minikit (QIAGEN).

Luciferase Assay

HEK293 cells were transfected using calcium-phosphate precipitation with the *CDK1* promoter reporter or the 6xDB reporter (FoxM1 DNA-binding motif). For NF45 or NF90-overexpressing cells, HEK293 were co-transfected with the *CDK1* promoter reporter or 6xDB reporter and NF45 or NF90. For NF45 or NF90-depleted cells, HEK293 cells were transduced with shNF45 or shNF90. Then, 24h post-selection, cells were transfected with luciferase reporters. 48h post-transfection luciferase activity was measured according to Secrete-Pair Gaussia Luciferase Assay Kit (Genecopoeia) and using the plate-reader Infinite 200 PRO (Tecan).

Generation of Stable Inducible Cell Pools and BioID Labeling

Parental HEK293 Flp-In T-Rex cells and cells expressing GFP-BirA R118G fused to flag tag were provided by Dr. Anne-Claude Gingras (University of Toronto, Toronto, Canada). Stable cell lines were generated in parental HEK293 Flp-In T-Rex cells expressing bait proteins of interest as described (Kean et al., 2012). Stable cell lines were selectively grown in the presence of 200 μg/mL hygromycin

up to 80% confluence before expression was induced using 1 μg/mL tetracycline for 24 hours. For the BioID experiments, 50 μM biotin was added at the time of induction. Two 150-mm plates were induced with tetracycline and treated with biotin for 24 hours before harvesting. Cells were pelleted at low speed, washed with ice-cold PBS and frozen at −80°C until purification. Cell pellets were thawed in 1.5 mL ice cold RIPA buffer containing 20 mM Tris-HCl (pH 8), 137 mM NaCl, 1% NP-40, 0.1% SDS and 0.5% sodium deoxycholate. 1 mM phenylmethylsulfonyl fluoride, 1 mM dithiothreitol and a complete protease inhibitor cocktail tablet (Roche) were added immediately before use, supplemented with 250U of benzonase. The lysates were sonicated using three 10 s bursts with 10 s rest in between on ice at 20% amplitude. Lysates were centrifuged for 20 min and cleared supernatants were transferred to 2 mL microcentrifuge tubes, and a 60 μL bed volume of prewashed streptavidin-agarose beads (GE Healthcare) was added to each sample. Affinity purification was performed at 4°C on a nutator for 3 hours, and the beads were washed twice in RIPA buffer, and three times in 50 mM ammonium bicarbonate (ABC; pH 8.0). After affinity purification and removal of all washing buffer, beads were resuspended in 100 μL of 50 mM ABC (pH 8) with 1 μg of trypsin (Sigma-Aldrich) added and incubated at 37°C overnight with agitation. The next day, an additional 1 μg of trypsin was added to each sample, and the samples were incubated for 4 hours at 37°C. Beads were pelleted and the supernatant was transferred to a fresh 1.5 mL tube. The beads were then rinsed two times with 100 μL of MS-grade H_2O, and these rinses were combined with the original supernatant. The pooled fractions were centrifuged, and the supernatant was transferred to a new 1.5 mL tube and dried in a vacuum centrifuge. Tryptic peptides were resuspended in 10 μL of 5% formic acid.

Mass Spectrometry Acquisition and Data Analysis

Samples were reconstituted in formic acid 0.2% and loaded and separated on a homemade reversed-phase column (150 μm i.d. x 150 mm) with a 56-min gradient from 0%–40% acetonitrile (0.2% FA) and a 600 nl/min flow rate on an Easy-nLC II (Thermo Fisher Scientific), connected to an Orbitrap Fusion Tribrid mass spectrometer (Thermo Fisher Scientific). Each full MS spectrum acquired with a 60,000 resolution was followed by 20 MS/MS spectra, where the 12 most abundant multiply charged ions were selected for MS/MS sequencing. Samples analyzed were converted to mzXML using ProteoWizard 3.0.4468 (Kessner et al., 2008) and analyzed using the iProphet pipeline (Shteynberg et al., 2011) implemented within ProHits (Liu et al., 2010). The database consisted of the human and adenovirus sequences in the RefSeq protein database (version 57) supplemented with "common contaminants" from the Max Planck Institute (https://maxquant.org/downloads.htm) and the Global Proteome Machine (GPM; https://www.thegpm.org/crap/index.html). The sequence database consisted of forward and reversed sequences. The search engines were Mascot (2.3.02; Matrix Science) and Comet (2012.01 rev.3 (Keller et al., 2002)), with trypsin specificity and two missed cleavage sites allowed. Methionine oxidation and asparagine/glutamine deamidation were set as variable modifications. The fragment mass tolerance was 0.01 Da and the mass window for the precursor was ± 10 ppm. The resulting Comet and Mascot results were individually processed by PeptideProphet and combined into a final iProphet output using the Trans-Proteomic Pipeline (TPP; Linux version, v0.0 Development trunk rev 0, Build 201303061711). TPP options were as follows. General options were -p0.05 -x20 -PPM -d"DECOY," iProphet options were pPRIME and PeptideProphet options were pP. All proteins with a minimal iProphet protein probability of 0.05 were parsed to the relational module of ProHits. Note that for analysis with SAINTexpress, only proteins with at least two peptides identify and with iProphet protein probability $\geq$ 0.95 are considered. This corresponds to an estimated protein level FDR of ~0.5%.

QUANTIFICATION AND STATISTICAL ANALYSIS

Student's t test was used for comparisons between two groups with at least n = 3. A p value < 0.05 was considered significant for all parameters tested. Error bars indicate standard deviation (s.d.). For Figures 2I–2L, one-way ANOVA was performed. All experiments were performed a minimum of three times. Statistical details for each experiment are located in the results, figures, and figure legends.

Cell Reports, Volume *31*

Supplemental Information

NF45 and NF90 Regulate Mitotic Gene Expression by Competing with Staufen-Mediated mRNA Decay

Sami Nourreddine, Geneviève Lavoie, Justine Paradis, Khaled Ben El Kadhi, Antoine Méant, Léo Aubert, Benoit Grondin, Patrick Gendron, Benoit Chabot, Michel Bouvier, Sébastien Carreno, and Philippe P. Roux

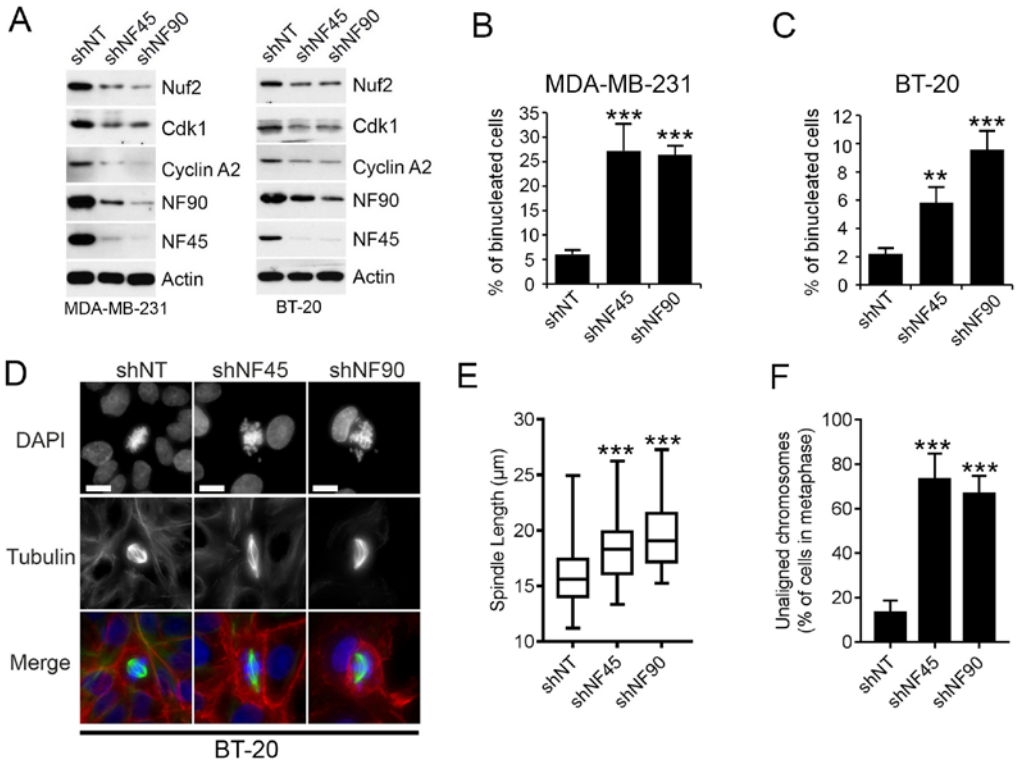

Figure S1
Nourreddine et al.

Figure S1. Impact of NF45 or NF90 depletion in breast cancer cell lines. (A) Triple negative breast cancer cell lines BT20 and MDA-MB-231 cells were depleted for NF45 or NF90 using shRNAs. Abundance of NUF2, CDK1, CCNA2 and Survivin were assessed by immunoblotting. **(B, C)** Quantification of binucleated cells by immunofluorescence in response to NF45 or NF90 depletion. A minimum of 1500 cells per condition was quantified. ***p<0.001 (two-tailed *t*-test) **(D)** BT-20 cells subjected to NF45 or NF90 depletion were stained for Tubulin (green), F-Actin (red) and DNA (blue) and imaged at 60x magnification. Scale bar 25 µm **(E)** Quantification of BT-20 cells metaphase spindle length. At least 25 cells per condition were analyzed. ***p<0.0001 (one-way ANOVA). **(F)** Quantification of BT-20 cells having unaligned chromosomes in metaphase. At least 50 cells per condition were analyzed. ***p<0.001 (two-tailed *t*-test). Related to Figure 3.

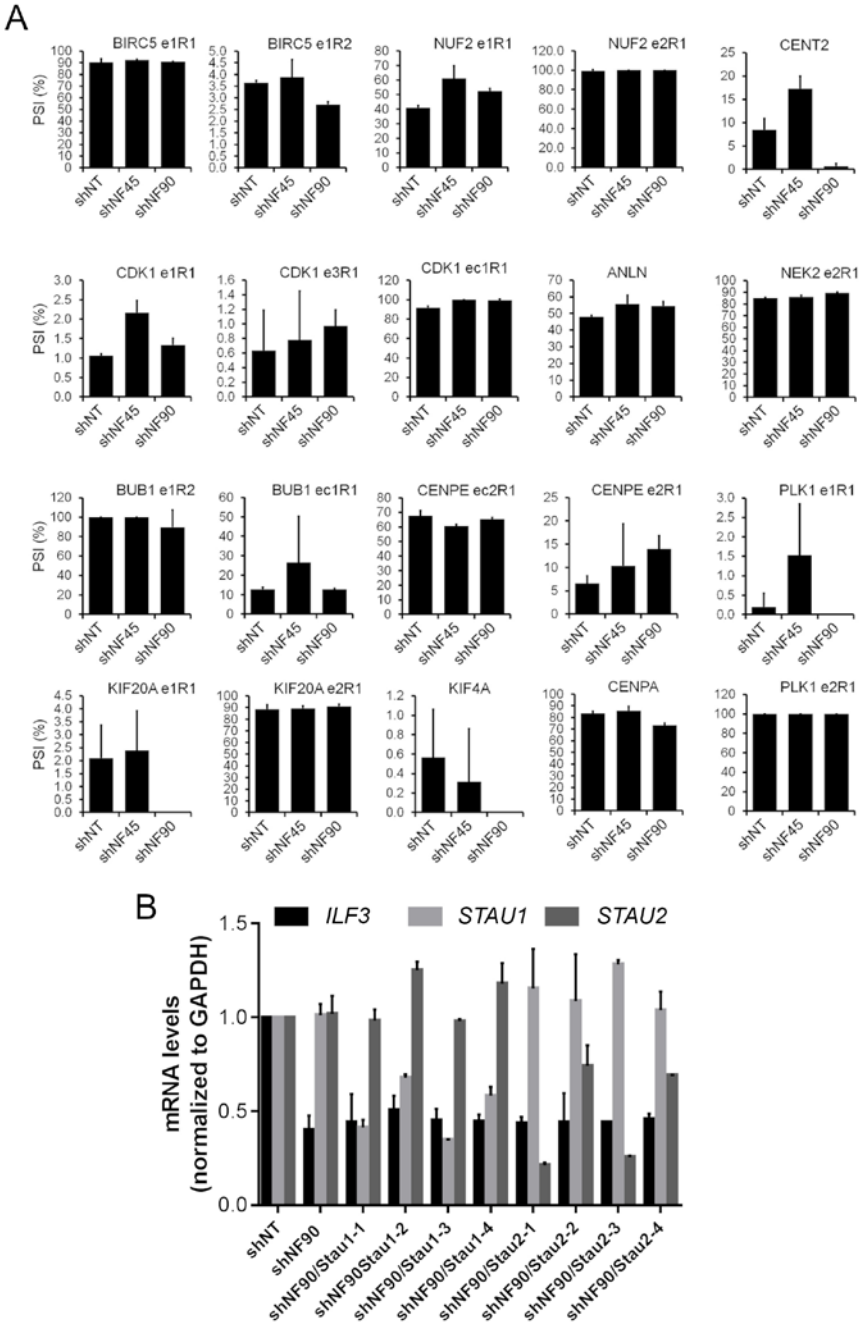

Figure S2
Nourreddine et al.

Figure S2. Analysis of mitotic gene alternative splicing in response to NF45 and NF90 depletion.

(A) HeLa cells stably expressing shNT, shNF45 or shNF90 were extracted for RNA and Alternative Splicing PCR was performed to quantify the different splicing isoforms of mitotic genes.

(B) qPCR of HeLa cells stably expressing shNT, shNF90, and combinations of shNF90/shStau1 or shNF90/shStau2 using 4 different shRNAs targeting Stau1 or Stau2. *ILF3*, *STAU1* and *STAU2* mRNA levels correspond to the conditions found in the functional assay perform in Figure 4F.

Related to Figure 4.

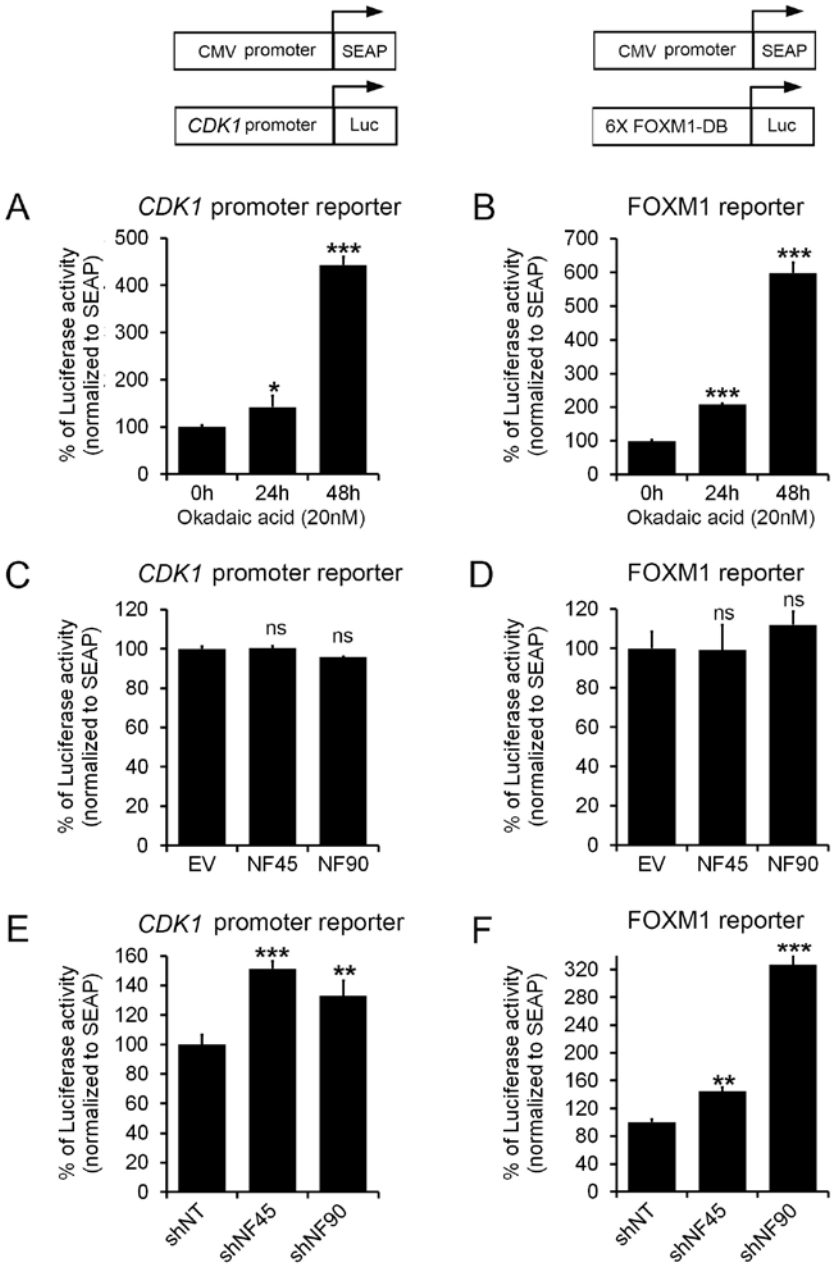

Figure S3
Nourreddine et al.

Figure S3. **Transcriptional regulation of mitotic genes in cells with loss- and gain-of-function in NF45 and NF90. (A, B)** HEK293 cells were transfected with plasmids encoding luciferase under the control of the *CDK1* promoter or 6x FoxM1 DNA-binding motifs, and treated with 20 nM Okadaic acid for 24h or 48h. *p<0.05 ***p<0.001 (two-tailed *t*-test). **(C, D)** HEK293 cells were co-transfected with NF45 or NF90 overexpressing vectors and plasmids encoding luciferase under the control of the *CDK1* promoter or 6x FoxM1 DNA-binding motifs. **(E, F)** HEK293 cells stably expressing shRNA targeting NF45 or NF90 were transfected with plasmids encoding luciferase under the control of the *CDK1* promoter or 6x FoxM1 DNA-binding motifs. **p<0.05 ***<0.001 (two-tailed *t*-test). Related to Figure 3.

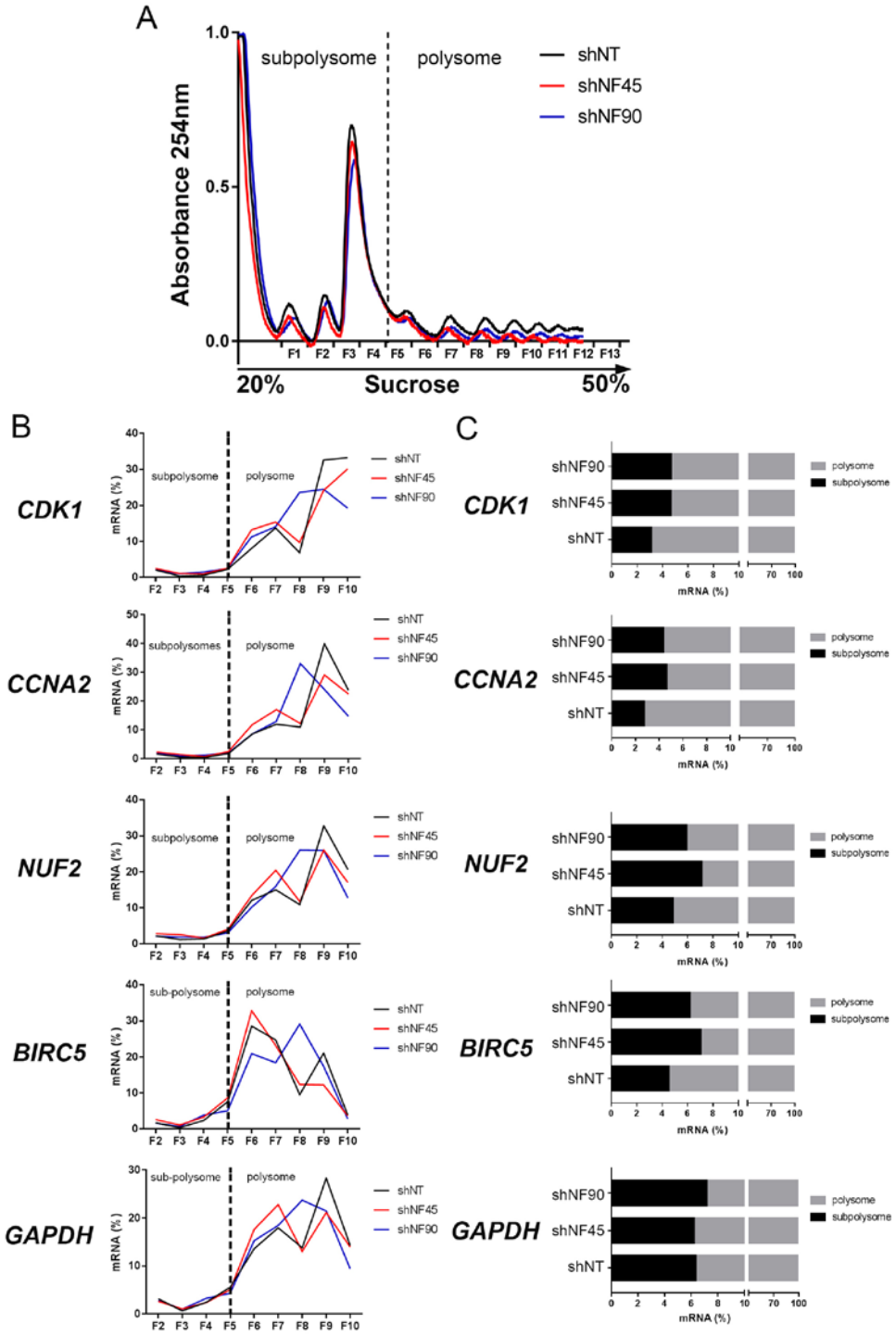

Figure S4
Nourreddine et al.

Figure S4. Translational regulation of mitotic genes in response to NF45 or NF90 depletion. **(A)** Ribosome profiling of HeLa cells stably expressing shRNAs targeting NF45 or NF90. **(B)** Relative distribution of *CDK1*, *CCNA2*, *NUF2*, *BIRC5* and *GAPDH* mRNA in the different ribosomal fractions. **(C)** Normalized distribution of *CDK1*, *CCNA2*, *NUF2*, *BIRC5* and *GAPDH* mRNAs in the subpolysome and polysome fractions. Related to Figure 4.

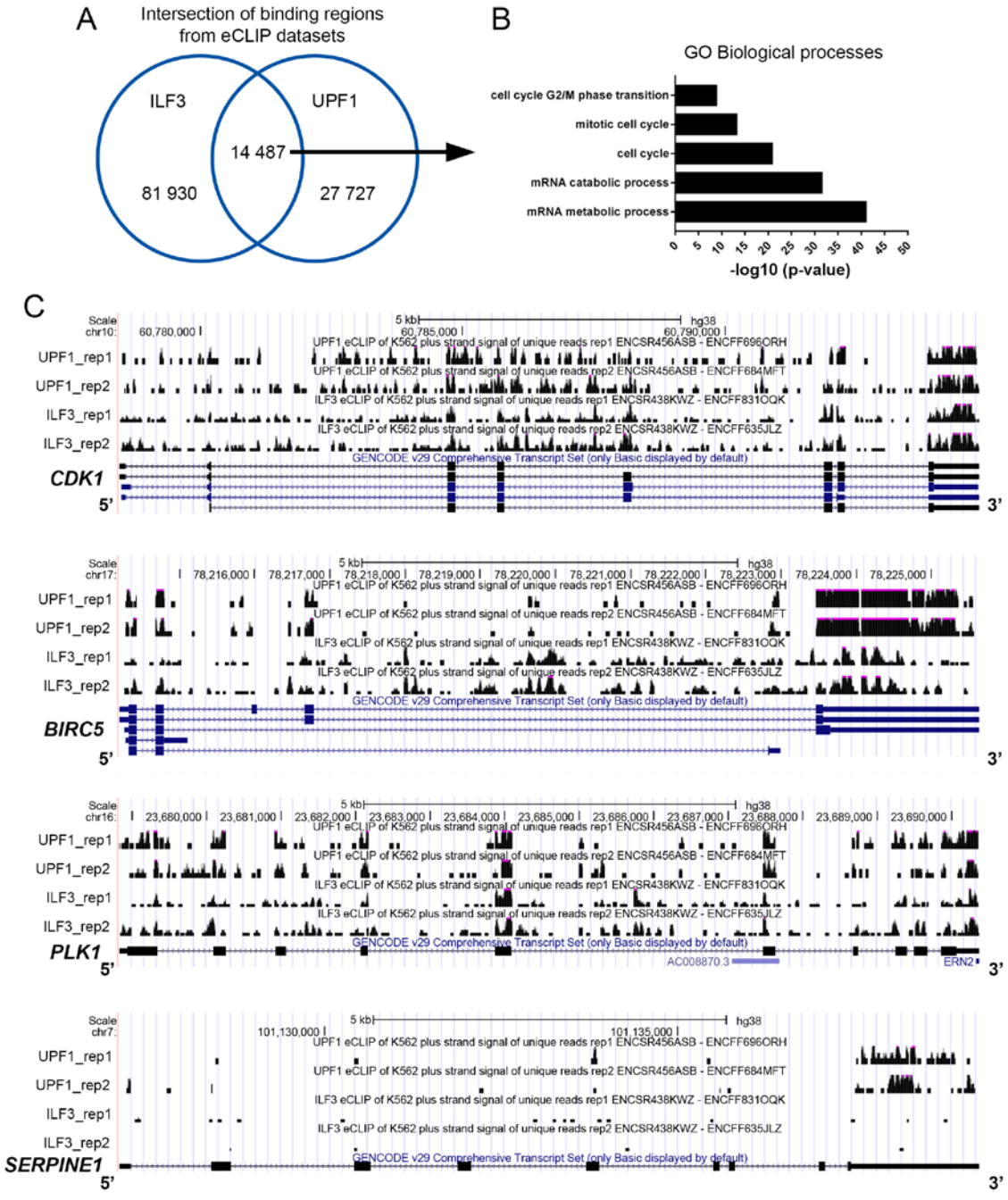

Figure S5
Nourreddine et al.

Figure S5. Intersection of NF90 and UPF1 binding regions on target mRNAs. (A) Overlapping binding sites between ILF3 (GEO: GSE91760) and UPF1 (GEO: GSE91776) eCLIP datasets from K562 cells obtained from the ENCODE database (www.encodeproject.org). **(B)** Gene Ontology analysis of overlapping peaks between ILF3 and UPF1 eCLIP datasets. **(C)** Representation of ILF3 and UPF1 eCLIP peaks on CDK1, BIRC5, PLK1 and SERPINE1 genes using the UCSC genome browser. Coding exons are showed by blocks connected by lines representing introns. 5' and 3'UTR are represented as thinner blocks on the leading and trailing ends of the genes. Related to Figure 4.

Table S4. List of all primers used for qPCR and ASPCR, Related to STAR Methods.

qPCR		
Gene	Primer Forward	Primer Reverse
ILF2	CCTGGTGGTGATACTCAAGATTC	CTTAGGCTTTCCACGACTTTG
ILF3	CTGGTGCTGCTGTGTAAGGA	TGCAGTATTTCGTACTTGTCTTCTG
NUF2	CCAGAAGCTTAAAAATGCCAGA	TGATATAACTGCACTTCCAACTGAC
CDK1	TGGATCTGAAGAAATACTTGGATTCTA	CAATCCCCTGTAGGATTTGG
CCNA2	CCATACCTCAAGTATTTGCCATC	TCCAGTCTTTCGTATTAATGATTCAG
BIRC5	CCGCATCTCTACATTCAAGAACT	GCCAAGTCTGGCTCGTTC
ATCB	ATTGGCAATGAGCGGTTC	TGAAGGTAGTTTCGTGGATGC
GAPDH	AGCCACATCGCTCAGACAC	GCCCAATACGACCAAATCC

ASPCR		
Gene	Primer Forward	Primer Reverse
ANLN	TGACCGAAAACCAGATACCAG	TCTCCTCTTGGCTCTTCTCCAT
BIRC5.1	TTCAAGGAGCTGGAAGGCTGG	CACAGGAAGGCTGGTGGCA
BIRC5.2	CCACTGAGAACGAGCCAGAC	GACAGAAAGGAAAGCGCAACCG
BUB1.1	GGACCCAGTTGATGGAAAGACT	AGGTCAATCAGTGCCAAGCCAG
BUB1.2	AGTTTGCGGTTCAGGTTTGGC	CTGATGAATCTTGGGTCATTGTGG
CDK1.1	CTTGGAAATTGAGCGGAGAGCG	TCCATAGTTAGTCAATGGGTATGGT
CDK1.2	TTGCTGAACTAGCAACTAAGAAACC	ACTTCATTATTGGGAGTGCCCA
CDK1.3	TGGATTCTATCCCTCCTGGTCA	TGGAGTTGAGTAACGAGCTGAC
CENPA	TTCCTCCCATCAACACAGTCGG	GCCAGTTGCACATCCTTTGGG
CENPE.1	GTTGAACTCACTTCGTGCTGAC	TCTGGTCTTCCTTTTCTCTAAGCAG
CENPE.2	GGAACTAAAAACTGCTCGTATGCT	ACTTGGTGGTTCTGTCGGTC
CETN2	AGGAAGGGACAGGAAAAATGAACT	CCAGTTTCATCATCATCAAAGAGCT
KIF20A.1	CCAGGAGGAGCAAGTGGCA	ACATCGTCATCGGACAGCAAG
KIF20A.2	TGAACATTTGGACACCCAAAAGG	ATCAATGGTGAAGGGCTTGGCT
KIF4A	GGGAGAACGGGGAAGGGACATT	CCAGAGGGCGACAACGCAGC
NEK2.1	TGGGCTGCTTGCTGTATGAGTT	CGCCTGAATTTGCCTTCTCTGA
NEK2.2	TACAGCTTGCTAAAGGAACGGA	TCATGATGTTCTCTTTACTTTCCCCA
NUF2.1	TGATGACGGTTGACGTTTGCTG	CTGGGGAAAGACAAAGTTTCCATC
NUF2.2	GGTCCAGAAGCTTAAAAATGCCA	TTTGAATTGTGCTGTGGCAAGT
PLK1.1	CGTGTTCGTGGTGTTGGAGC	ATTTGCCGTAGGTAGTATCGGG
PLK1.2	CCCGATACTACCTACGGCAAAT	CTGTGCCCTTTCTTGCTCAGC
PLK1.3	CGTGCAGATCAACTTCTTCCAG	CTCAGGCGGTATGTGCGGAA